2D CMUT ARRAY BASED ULTRASONIC MICROMANIPULATION OF PARTICLES

A THESIS SUBMITTED TO

THE GRADUATE SCHOOL OF

ENGINEERING AND NATURAL SCIENCES

OF ISTANBUL MEDIPOL UNIVERSITY

IN PARTIAL FULFILLMENT OF THE REQUIREMENTS FOR

THE DEGREE OF

MASTER OF SCIENCE

IN

ELECTRICAL, ELECTRONICS ENGINEERING AND CYBER SYSTEMS

By

Arooba Zeshan

August, 2017

ABSTRACT

2D CMUT ARRAY BASED ULTRASONIC MICROMANIPULATION OF PARTICLES

Arooba Zeshan

M.S. in Electrical, Electronics Engineering and Cyber Systems

Advisor: Assist. Prof. Feysel Yalcin Yamaner

August, 2017

Capacitive micromachined ultrasonic transducers (CMUTs) have gained increased attention in recent decades because of the advantages they hold over the conventional technology. The thesis introduces a concept of integrating row column addressed CMUT arrays with microfluidic channel to enable trapping and two dimensional manipulation of micro-particles.

Acoustic tweezers have several applications in different fields of science as they enable non-invasive and non-contact manipulation of microparticles. The current strategies of designing and implementing acoustic tweezing involve piezoelectric (PZT) materials for transduction mechanism. However, PZTs impose certain limitations on particle handling, such as long operating time could heat up the microfluidic channel that could disturb the specimen's viability. They also require a matching layer for proper coupling of acoustic energy into the channel, which adds to the complexity and over all cost of the devices.

The CMUT technology has several advantages over the conventional technology, for-example, flexibility while optimizing the design parameters, easy fabrication techniques and low self-heating during continuous operations. CMUT overcomes the difficulties in miniaturization, providing smaller transducer arrays and these arrays can conveniently be fabricated on chip without requiring matching layer.

Finite element analysis (FEA) was used to optimize the transducer's characteristics. Based on the parameters of one CMUT cell, an array was modeled that was integrated with a microfluidic channel. The design strategy was to model a half wavelength resonator, where the thickness of the channel was kept as half wavelength corresponding to the resonance frequency. A glass reflector was finally modeled on top of the fluid channel. On resonance, a standing wave was generated that dragged the particles towards the pressure field minima. The results of FEM simulations depicted the acoustic potential minimum and hence the trapping site of the particles. Acoustic radiation forces were then calculated

based on the results of the analysis. A row column (RC) addressed CMUT arrays were also drawn to depict the effect of non-active elements on the pressure field. After optimizing the design parameters of the device, RC CMUT arrays were then fabricated by employing anodic bonding. This method has many benefits over the fabrication techniques found in the literature, for-example, easy and simple fabrication processes, high fill factor and effective membrane uniformity. In this approach brosilicate glass is used as a substrate which effectively reduced the parasitic capacitance and thus improved the sensitivity of the devices.

ÖZET

2D CMUT DİZİSİ KULLANILARAK PARÇACIK MİKROMANİPÜLASYONU

Arooba Zeshan

Elektrik-Elektronik Mühendisliği ve Siber Sistemler, Yüksek Lisans

Tez Danışmanı: Yrd. Doç. Feysel Yalcin Yamaner

Ağustos, 2017

Mikro parçacıkların yakalanmasını ve iki boyutlu manipülasyonunu sağlamak için sıra sütunlarına adreslenmiş CMUT dizilerinin mikroakışkan kanal ile birleştirilermesi tezin temel konusunu oluşturmaktadır. Bu çalışmada hedef frekansı 2.5 MHz olan çok katmanlı düzlemsel bir rezonatör tasarlanmış ve simülasyonları yapılmıştır. Sonlu elemanlar modellemesi ve simülasyonları ile bir parçacığın CMUT'i aktive ederek sıvı kanalı içindeki hem yanal hem de eksensel yönlerde sıkıştırabileceği ve manipüle edilebileceği gösterilmiştir. Önerilen platform ile 10μm yarıçapında bir polistiren parçacığına etki eden akustik radyasyon kuvveti, FEM sonuçları kullanılarak hesaplanmıştır. Optimize edilmiş parametrelere dayanarak, anodik yapıştırma teknolojisini kullanarak bir cam taban üzerinde 32x32 elemanlı sıra / sütun adresli 2 boyutlu CMUT dizisinin üretimi gerçekleştirilmiştir. Bu yaklaşım, mikro parçacık tutma ve işleme için kolayca uygulanabilir düşük maliyetli ve etkin ve bir çüzüm sağlamaktadr.

Anahtar sözcükler: CMUTS, RC, FEM.

Acknowledgement

I would like to express my deepest gratitude to my supervisor Dr. Yalcin Yamaner, for introducing me to this interesting field and guiding me through out this degree. I am very thankful to him for always being so helpful and encouraging.

I am thankful to my thesis committee members, Dr. Mehmet Kocaturk and Dr. Burcu Saner Okan for taking time out from their busy lives to review the thesis. I am very grateful to Prof. Ömer Oralkan for his valuable advice and suggestions. My sincere thanks to Xiao Zhang, at North Carolina State University, for fabricating the devices.

Lastly I would like to thank my husband for his kind support throughout my MS program.

Contents

List of Figures

xi

List of Tables

Chapter 1

Introduction

Ultrasonic transducers deploy various physical mechanisms that transform electrical energy to acoustic energy and conversely acoustic energy to electrical energy. Among them some of the commonly used mechanisms are piezoelectricity and electrostatics. For decades piezoelectric ceramics and crystals have been used for transduction mechanism and are commercially very easily available. The basic concept of capacitive micromachined ultrasonic transducers (CMUT) is almost as old as the idea of piezoelectric transducers, however, they could not gain much attention because of the high electric field that is needed to be maintained in order to achieve adequate efficiency. The recent growth in micro-fabrication technology has allowed sustaining electric fields of over 10^8 V/m. The research on these devices have rapidly developed ever since, leading to innovative and better approaches for designing, modeling and fabricating the transducers.
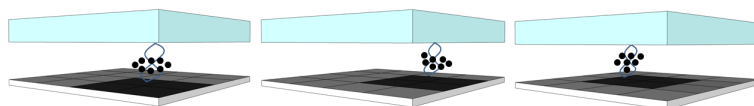
Figure 1.1: Planar acoustic resonator system incorporated with row column addressed CMUT arrays that allowed 2D manipulation of particles in the fluid channel.

The motivation behind this dissertation is to design and develop a 2D row column addressed CMUT array, that has been incorporated in a planar resonator system for particle trapping and manipulation using ultrasound waves, shown in Fig. (1). This design would allow microparticles handling in two dimensions. The existing techniques of handling and manipulating particles using acoustic waves (acoustic tweezers) is done by mechanically translated focused single-element transducers or generating standing wave patterns. However, it is not possible to generate complex patterns and arbitrary manipulate more than one particle in parallel using these devices. Also, almost all of the techniques deploy PZTs to generate the required sound waves. In this thesis it was shown that the use of CMUTs as transducers overcome several limitations imposed by the PZTs transducers and are also a cost-effective and simple approach that can easily be implemented in a lab environment.

In this work a finite element analysis of the design was performed using ANSYS Mechanical APDL. The transducers parameters were optimized in a way that they would create enough acoustic radiation force required for trapping and manipulating a micro-particle. The FEM results show the trapping position of the particles and the forces on the particles are also calculated using the same model. The row-column (RC) addressed CMUT arrays were then fabricated, using the parameters found during finite element modeling. The fabrication is done by anodically bonding borosilicate glass with SOI wafer. The fabrication technique is simple, cost-effective and takes care of parasitic capacitance issue that was found in previous implementations.

The thesis is organized as follows: an introduction on capacitive micromachined ultrasonic transducers is given in Chapter 2 along with an evolution of this technology with time. In Chapter 3, comprehensive details on micro-particle manipulation are presented. Chapter 4 consists of the finite element modeling of the suggested design and the fabrication of the CMUT devices is presented in Chapter 5. Finally, the thesis is concluded with Chapter 6, that includes discussion based on findings.

Chapter 2

Background Theory

This chapter serves to give a brief introduction on piezoelectric transducers and their limitations and how CMUTs overcome those shortcomings and emerge as a powerful tool for generating acoustic waves. The design details are given in this chapter along with the a comprehensive literature review on the evolution of the devices.

2.1   Piezoelectric Transducers

Piezoelectric transducers operate on the principle of piezoelectric effect, which is the ability of a material to generate electric charge when mechanical stress is applied to it, and conversely results in mechanical vibrations when placed in an electric field. The most commonly used material for medical transducers is the ceramic poly crystalline lead-zirconate-titanate (PZT) [1]-[2].

Despite being commercially popular for decades, piezoelectric transducers have some limitations. One of them is the acoustic impedance miss-match between the piezoelectric layer (impedance (Z) is greater than 30 MRayl for conventional PZT) and the medium, such as air (Z $\approx$ 400 Rayl), water (Z $\approx$ 1.5 MRayl), or soft tissues (Z $\approx$ 1.6 MRayl). A matching layer is therefore required for proper

coupling of acoustic energy into the medium [3]-[4]. The matching layer, also called acoustic transformer, does not ensure 100% transmission and the reflected waves echo inside the PZTs, which gives rise to the need of having a backing layer. These layers add to the complexity and hence the overall cost of the devices. These layers play a critical role in the design of acoustic resonators, as studies suggest that zero matching layer is optimum for the design of acoustic tweezers [5].

Another limiting factor of PZTs lies in the fact that the thickness of the devices determines their operating frequencies and, therefore, fabrication complexity increases and efficiency degrades for high frequency designs. Also, heat is generated within the PZTs due to the electrical and mechanical losses which invoke the risks of unstable performance, a rise in temperature and even degradation of the devices. Use of PZTs could, therefore, damage the specimen if operated for a longer period of time.

These shortcomings encouraged researchers to move their focus to capacitive micro machined ultrasonic transducers, that do not only overcome these shortcomings but have also brought revolutionary changes in the field of ultrasound [6].

2.2 CMUTs

CMUTs are based on the principle of electrostatic transducers, where the transduction mechanism is the vibration of thin plates under electrostatic force. Many examples of such transducers exist in macro-scale such as electret condenser microphone. The advancement in semiconductor fabrication technologies has made possible the fabrication of CMUTs, which are essentially MEMS based electrostatic transducers working in ultrasonic frequencies.

The thin plate of the CMUT results in low mechanical impedance and hence provides better acoustic impedance matching to the medium and does not require matching layers. The fabrication techniques make CMUTs a promising option for the generation of acoustic waves as they make use of the well known and well developed techniques of integrated circuit (IC) processing to fabricate different transducer arrays, with various shapes, sizes and resonant frequencies, on

one wafer which can easily be incorporated with electronic circuit either mono-lithically or by flip-chip bonding. Because CMUTs are fabricated from highly thermally conductive silicon, therefore, they can be operated for a longer period of time without suffering from self-heating. These benefits make CMUT well suited for imaging, therapy and sensing applications.

2.2.1 Design and Structure

Fig. 2.1 shows the fundamental structure of a CMUT cell. Basically, the design of a CMUT cell consists of a parallel plate capacitor, with the bottom electrode rigidly placed and the top electrode residing on a flexible membrane. The main purpose of the membrane is to transmit and receive an acoustic wave in the adjacent medium. For operating CMUTs, the membrane is deflected by applying a bias voltage between the two electrodes, which deflects the top plate towards the bottom plate due to an electrostatic force, making it more sensitive to any additional forces, be it electrostatic force or external force due to pressure.
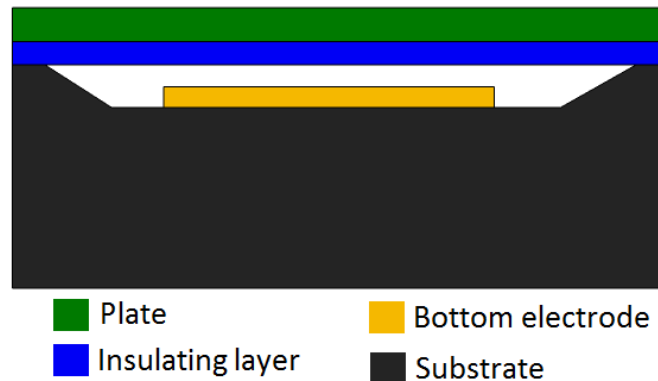
Figure 2.1: Schematics of a CMUT cell

The generated electrostatic force is proportional to the area of the capacitor, the square of the applied voltage, and the permittivity of the material between the plates, and inversely proportional to the square of the gap between the two electrodes:

$$F = \frac{\epsilon A V^2}{2d^2} \qquad (2.1)$$

where A is the area of capacitor plates, V is the applied bias voltage, ϵ is the permittivity of free space between capacitor plates, and d is the gap between them.

If an alternating voltage is superimposed on the bias voltage, such that $V = V_{ac} + V_{dc}$, the electrostatic force results in the vibration of the membrane which results in the generation of ultrasound waves.

$$F = \frac{\epsilon A}{2d^2}(V_{dc}^2 + 2V_{dc}V_{ac} + V_{ac}^2) \qquad (2.2)$$

Conversely an incoming ultrasonic wave causes the plate to vibrate, changing the capacitance of the cell which results in current that can be detected by an electronic circuit. The capacitance, C, is related to the charge q, and voltage V, through the equation:

$$C = \frac{q}{V} \qquad (2.3)$$

And hence the amplitude of the detected current depends on the bias voltage and capacitance of the device.

If the bias voltage on the CMUT is increased the gap between the two electrodes decreases which in return increases the electrostatic forces. When the electrostatic force gradient becomes larger than the mechanical force gradient the top electrode collapses on to the bottom electrode. The bias voltage at which the membrane collapses is called the collapse voltage or pull-in voltage of the device.

2.2.2 Modes of Operation

CMUTs can be operated in two regimes: conventional and collapse. In conventional mode of operation, the transducer is biased at a voltage that is close to the collapse voltage, 80% of it. The bias voltage and alternating voltage are adjusted

so that the two electrodes do not come in contact with each other.

Another operating regime, proposed by [7], where the membrane is first biased at a voltage higher than the collapse voltage, that collapses the membrane onto the substrate. The bias voltage is then reduced to a voltage between the collapse and snap back voltages. At this operating voltage, the center of the membrane still contacts the substrate. By adding an AC voltage, harmonic membrane motion is obtained at a circular ring concentric to the center. The operation enables high volumetric displacement thus increasing the output pressure. Collapse mode operation is not suitable for particle manipulation due to nonlinearity and uncertainty of snapback motion.

2.2.3 Literature Review

The CMUT technology has evolved to a large extent ever since the first devices developed by the research group of Stanford, E.L. Ginzton Laboratory (Stanford, CA, USA). The initial papers, authored by Haller and Khuri-Yakub, describe basic principles of micromachined transducers and how the devices can be fabricated by the use of sacrificial oxide etch to form the cavities [8] [9].

In 2002, Omer Oralkan et. al demonstrated that CMUTs can be effectively incorporated as 1D and 2D linear arrays [6], and have also shown the operation of devices in high frequencies, 60MHz in air and 45MHz in immersion [10].

The CMUT technology particularly holds many applications in medical ultrasound imaging. It was shown through experiments in [11] [12] that the imaging results by using CMUTs are not just comparable to the conventional technology but render better image quality.

Apart from imaging CMUTs have also been deployed in many different applications. In [13] a therapeutic ultrasound chip was developed which was monolithically integrated with a silicon substrate along with an imaging CMUT. This configuration allowed real time imaging of the targeted object.

Wong et al. designed and developed an eight element concentric ring CMUT

array to treat upper abdominal cancer cells, in another high intensity focused ultrasound (HIFU) example [14]. In [15] a 2D CMUT array that was calibrated and packaged as a hydrophone was developed with integrated front-end electronics. The technology has also been deployed in applications where they were used as mixers for lab-on-a-chip experiment [16] and as acoustic receiver for photo acoustic imaging [17] and more recently CMUT array were used as tunable acoustic metamaterials by [18].

Researchers have also been investigating air coupled transducers where authors of [19] used CMUTs for defect imaging in aluminum and composite plates. Wang et al reported a CMUT based air coupled transducer for non-destructive evaluation with higher transduction efficiency than the conventional methods [20].

The CMUT technology also holds applications as chemical sensors [21] [22], where they create a low noise oscillators by electrically connecting multiple CMUT cells that aimed to improve the sensitivity of a chemical sensor.

2.2.4 Finite Element Analysis

As the CMUT technology has improved over time and has been deployed in several different applications, the techniques to optimize the devices with improved efficiency has advanced as well. Finite element analysis has been an integral part in designing CMUTs and to understand the transducer characteristics and optimize the transducer response [23]. To avoid the costs and complexities of fabricating the devices, the simulations are necessary that can predict the behavior of the sensors beforehand.

Bozkurt et al. used finite element analysis and normal mode theory to investigate the structural loss mechanism of CMUTs. They reported that the losses are due to the radiation of energy which is coupled to the silicon wafer at their intersection. This analysis was used to adjust the membrane parameters to tackle these losses and reduce cross-coupling [24].

Bozkurt et al. later used electrode patterning in finite element analysis to optimize the performance of a circular immersion CMUT membrane. They showed the bandwidth increases by a considerable amount by using an electrode which

8

is 40% to 50% the size of the membrane.

Baris Bayram et al. used finite element analysis to model a circular membrane and investigated the effect of electrode parameters on the collapse voltage, with constant metal plate thickness, and reported that the collapse voltage for half metallized structures and full metallized structures are almost equal [25].

Baris Bayram et al. later reported the collapse based operating regime of the CMUTs, which was mentioned earlier in this chapter. The finite element analysis results showed that the devices operating in this new regime possess a coupling coefficient (k_T^2) higher than a CMUT operating in the conventional regime [7].

Roh et al. analyzed the cross-talk within the CMUT cells element and between array elements, which could not be previously predicted by the Mason type equivalent circuit model as it ignored the effect of coupling to the substrate and also lacked the ability to predict cross talk. They also investigated how the effect of cross talk can be minimized by changing the thickness of the devices or by varying the structure of the silicon wafer [26].

CMUTs for air coupled applications were characterized by creating an axis symmetric finite element model (FEM) of a CMUT cell that accounted for the nonlinear effects of the device when the membrane deflects more as compared to its thickness. They fabricated two designs based on those FEM results [27].

In this work, finite element methods were used to characterize the devices and optimize the response of a half wavelength acoustic resonator. The devices were fabricated based on FEM results.

2.2.5   Fabrication Techniques

A very rapidly advancing topic in the research of CMUTs is how these devices are fabricated. The earlier devices were fabricated using a sacrificial release surface micro-machining technique and this process has been used for over a decade to fabricate CMUT devices. Another fairly popular technique of fabrication is the wafer bonding technique proposed by Huang et al [28]. Mostly all devices are fabricated by modifying the aforementioned techniques. Both of them have their pros and cons, which are discussed in detail below:

2.2.5.1 Surface micro-machining methods

The basic principle of surface micro-machining is to use a sacrificial layer on the carrier substrate to form cavities underneath the membrane. The sacrificial layer is selectively removed by using an etchant, which is chosen such that it only removes the sacrificial layer and not the membrane layer. The popular materials that have been used as a sacrificial layer are poly-silicon and the membrane layer is silicon nitride while properly doped silicon is usually chosen as a substrate.

The fabrication method is basically the same as describe by [29], and is illustrated in Fig. 2.2

The process begins with an electrically conductive silicon wafer, which acts as a bottom electrode for the entire transducer. The insulating layer is deposited, which also acts as an etch stop layer during sacrificial release, using LPCVD. The thickness of the layer is adjusted so as it is thick enough to protect the silicon wafer from the etchant but not too thick that could cause the active capacitance of the device to decrease.

The sacrificial material, such as chrome and polysilicon, is then deposited. To achieve lower height of the etch channels as compared to the height of the cell cavities, the material is often deposited in two steps. Hence an extra photolithography, etch and second sacrificial layer deposition steps are required. This is done because lower heights of etch channels are easier to seal in the final steps of the fabrication.

The cell cavities and membrane shape are then patterned on the sacrificial layer using another photolithography step. The membrane can be of any shape but the most commonly used shapes are circular and hexagonal. The membrane layer is then deposited in two steps because the membrane material is also used to seal the etch channels. Etch channels allow the flow of etchants during membrane release, which are patterned using lithography. If the channels are designed properly, the size of the cavity does not change in the final sealing process. The sacrificial layer is then removed using wet etching. The channels available for etchant to get into the cavity are small therefore this process can take days to complete. After this step, the etch cavities are sealed with the same material as the membrane. The cavities are sealed with low pressure chemical vapor deposition (LPCVD), so that
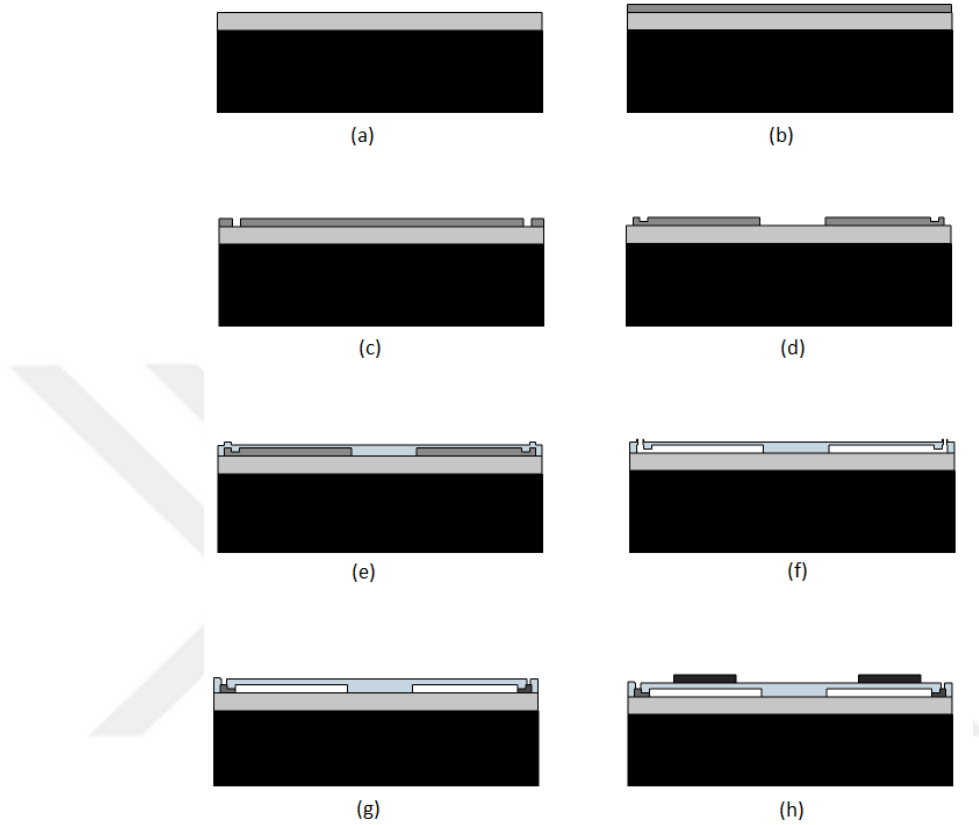
Figure 2.2: Fabrication steps of sacrificial release method: (a) deposition of insulation layer (b) deposition of the sacrificial layer (c) etch channels definition (d) formation of cavities and membrane (e) deposition of membrane materials (f) releasing membrane (g) sealing etch channels (h) exposing bottom electrode and metal deposition for contact pads.

there is no air left in the cavities. In the next step, the bond pads for the bottom electrodes are established using photolithography and are dry etched to access them. In the final step, the electrical connections are provided for the top and bottom electrodes using a lift off metal process.

Despite being popular for years, this method has some drawbacks. This process results in a poor control over thickness of the deposited layers, because the insulation layer, sacrificial layer and the plates are mostly created by using chemical vapor deposition (CVD). As the plate thickness is limited by the CVD process, hence CMUTs with thick plates can not be easily achieved. Another draw back of this process is the overlap of top and bottom electrodes at the posts. This overlap increases the parasitic capacitance. Also the etch holes take a large area

between the adjacent membranes which impose limitations on the active cells per unit area. This in turn limits the fill factor and results in a large amount of inactive region. Another drawback of sacrificial release method is a commonly occurring phenomenon called stiction. Stiction is caused by the large capillary forces that arise while drying the cavities after the removal of sacrificial material [30].

2.2.5.2 Wafer Bonding

Another popular technique for fabricating the CMUT devices is the wafer bonding processes. The three basic techniques of wafer bonding are anodic bonding, fusion bonding and adhesive bonding. Wafer bonding holds many advantages over the sacrificial release process, among which the main advantage is the simplicity of the process. The number of masks used are just four and there are only two deposition steps in the entire fabrication method. The fabrication flow is given in Fig. 2.3

Wafer bonding gives a very precise control over the thickness of the devices, as thermal oxide growth is very uniform. Also, without the need for sacrificial release channels the cells can be packed closer together which results in an increased fill factor and lower inactive region. The fill factor is critical at high frequencies, where elements are small and space is important in that case [10].

The fabrication process of fusion bonding, as given by [28] starts with two wafers, one is the silicon wafer and the other one a silicon on insulator (SOI) wafer. The two wafers are bonded in a vacuum environment to create the final device. Before the bonding, however, both wafers are separately treated. A thin silicon dioxide layer is grown on the top wafer and by using LPCVD an additional layer of silicon nitride is deposited on top.

Meanwhile, on the bottom wafer the cavities are etched by using reactive ion etching (RIE). The two wafers are thoroughly cleaned and are brought together in vacuum and annealed at 1100° to form a permanent bond. The box and handle layers of the SOI are then removed to release the membrane. In order to form the top electrode, a patterned metal layer is deposited using sputtering of aluminum.

Finally, the pads are opened for wire bonding.

The drawback of wafer bonding is that it results in an increased parasitic capacitance in the devices and hence degrades their performance. The parasitic capacitance is caused by the overlap of the substrate and the post regions. A way to tackle this is to use anodic bonding, where a bottom electrode, with defined cavities, is anodically bonded with SOI wafer. This process holds the benefits of wafer bonding, e.g. it is simpler, gives good control over thickness of the devices and high fill factor. The temperatures are also lower in anodic bonding as compared to fusion bonding and also gives relaxed surface roughness requirements [31].

In this dissertation, the devices are fabricated using anodic bonding, due to its
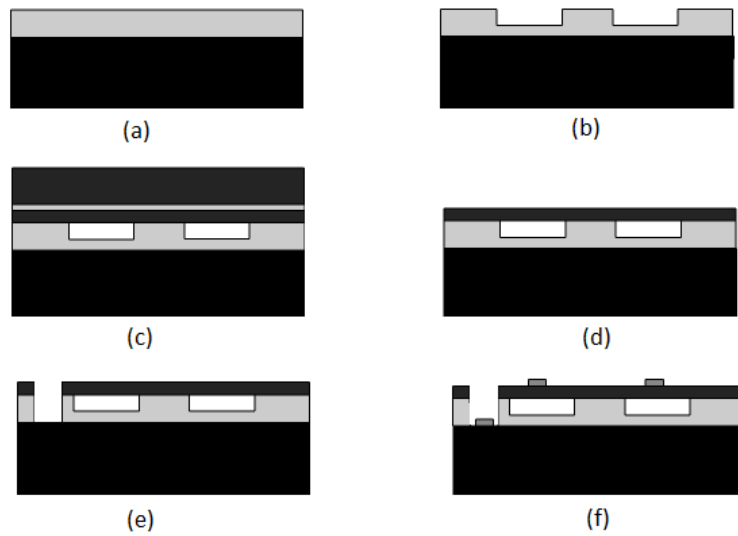
Figure 2.3: Fabrication steps of fusion bonding: (a) growth of thermal oxide for insulation and cell side walls (b) etching the cell cavities (c) fusion bonding the SOI wafer to the bottom wafer (d) release the membrane (e) expose the bottom electrode contact pad. (f) metalize the contact pads and top electrodes

advantages and simplicity. The three mask fabrication process that was deployed is given in detail in the following chapters.

Chapter 3

Particle handling and manipulation

Studies and research related to cells are carried out with an immensely large population of cells, the result, therefore, is an average value which is taken by calculating the response of more than one cells. This approach leads to misinterpretation as it fails to take into account the statistical behavior of several cellular level events. Hence, to obtain a statistically meaningful data it is important to conduct studies on one or on a sufficient number of cells.

Optical tweezing or laser trapping has been used for decades where a highly calibrated laser beam is utilized for particle trapping and handling. However, there is a certain criterion that needs to be fulfilled for laser trapping such as: the targeted specimen should be transparent, it should be non-absorbing at the wavelength of the trapping laser, also the refractive index of the particle should be different from that of the surrounding medium. When a laser beam interacts with the particle, it transfers its momentum to that particle and applies two forces on it: the scattering force, and gradient force. Where the former drives the particle in the direction of the light propagation and the latter pulls the particle in the direction of the field gradient. To obtain a stable trap the gradient force should be higher than the scattering force. The trapped particles can be handled in three dimensions by manipulating the laser beam and by changing the focus of

the beam. Dimensions of the particle that can be manipulated with laser ranges from a few Angstrom up to 10-μm [32] and the maximum trapping forces of up to hundred pico Newton can be acquired.

Laser trapping has been employed by many researchers to successfully trap and manipulate particles. In [33] the benefits of laser trapping were combined with hydrogel, that was sensitive to the change in temperature, and isolated a single yeast cell in a microfluidic channel. Arai et al. also presented another example of particle manipulation with high precision by using laser trapping, where they successfully attempted to tie knots on different biofilaments [34]. The filaments were attached with a polystyrene bead on each end and were trapped using two optical tweezers. Where one kept the biofilament in place and the other optical tweezer was manipulated in a way so as to tie a knot. The use of optical tweezers, however, has been restricted particularly in applications that require longer holding time as the intense trapping light could damage the biological structure and could also damage the trapped specimen through a process known as photo-damage [35].

Micro-electro-mechanical systems (MEMS) technology has facilitated this study and provided means to perform biological and chemical experiments on single molecules and single cells by creating tools that match the dimensions of cells and enables cell-handling.

3.1 Microfluidics

The advancement of MEMS technology brought revolutionary changes in various fields of science. The applications of MEMS devices surround us in our daily lives e.g inkjet printers, airbag deployment system in automobiles etc. The fabrication techniques have also evolved over time which laid the foundation of microfluidics. The field of analytical chemistry, first demonstrated the advantages of scaling down liquids into micro-channels for separation processes [36]. Since then, novel tools have been developed for studying molecules on a cellular level. Some of the main applications of microfluidics systems are: biological and chemical sensing, molecular separation such as DNA analysis, drug delivery etc. Microfluidics has

particularly benefited the cell based studies by translating it to lab on a chip domain which led to a cost-effective, simple and portable solution for particle handling and manipulation.

The concept of micromanipulation involves suspending the targeted particles in the microfluidic channel and non-inertial force fields, magnetic force [37], dielectrophoretic [38] and acoustophoretic forces [39], are applied to trap the targeted particle.

3.1.1 Magnetic Forces

Magnetic separation and sorting of cells have been increasingly applied in microfluidics to handle particles based on their magnetic susceptibility, which was first reported by [40]. In this technique, the microfluidic channels are actuated with permanent magnets [41] or with electromagnetic coils [42] which are either fabricated with the microchip or placed outside it. The suspended particles are then subjected to a non-uniform magnetic field because of which they experience a gradient force depending on various parameters such as: particle's volume, the magnetic susceptibility of the particle as compared to the medium as well as the gradient and strength of the magnetic field. Particles are attracted towards field maxima or minima based on their permeability.

The advantage of using magnetic manipulation is that factors such as surface charges, medium conductivity, temperature, does not influence particle manipulation. This technique gives good control over cell sorting and has been used in many different applications such as: CTC isolation [43], CTC capture [44], single cell isolation and analysis [45], isolating peripheral lymphocytes [46] and removal of malaria infected red blood cells [47]. However, magnetic fields are often improved by modifying properties of the medium [48] [49] or label [50] [51] objects of interest with magnetic particles to generate enough forces required for their handling.

3.1.2 Dielectrophoresis

In the vicinity of an inhomogeneous electric field, different polarizable particles, such as, cells, viruses, proteins, or DNA molecules, experience a dielectrophoretic (DEP) force. Dielectrophoresis technique uses this principle to trap and manipulate particles in the microfluidic channel. The non-uniform field is generated by fabricating arrays of insulating posts in the microchip. The particle or cell is either attracted towards regions of strong electric fields or is repelled from these regions which is determined by the polarizability of the suspended particle as compared to the medium.

Many research groups have used this technology for different applications such as trapping, focusing, fractionation of particles [42] [52] [53] [54] [55]. Hu et al. used this technique to sort cell by labeling them with polymeric beads and showed that cells that are bounded have higher DEP response amplitude unbounded cells [56]. Despite its popularity and simplicity, there are some drawbacks that limit its applications. For example the presence of strong AC fields causes Joule heating which leads to the setup of a transmembrane voltage and could also disturb the particles viability.

3.2 Acoustophoresis

Acoustophoresis, also known as acoustic tweezing, is the the manipulation of particles using acoustic waves, typically in the frequency range of 1MHz-10MHz. Kundt and Lehmann reported the effects of traveling acoustic waves which led to the earlier investigations of acoustic tweezing [39]. A sound wave traveling in one direction is defined by the acoustic pressure amplitude p_a, the frequency f corresponding to the angular frequency $\omega = 2\pi f$ and the wavelength λ. A plane traveling sound wave, in the positive z direction is then defined as:

$$p(z,t) = p_a sin(\omega t - kz) \tag{3.1}$$

where k is the wave number given as $2\pi/\lambda$. When two traveling waves with same frequencies and magnitudes but opposite in direction interact with each other

then that results in the generation of an ultrasonic standing wave (USW). USWs are, therefore, produced by the continuous superimposition of traveling waves with their reflection waves.

$$p(z, t) = p_a sin(\omega t - kz) + p_a sin(\omega t + kz) = 2p_a sin(\omega t)cos(kz) \qquad (3.2)$$

In Equation 3.2 the positions where the value of $z = n\lambda/2$, (n = 0, 1, 2 . .) amplitude is zero and these positions are called nodes and the positions where $z = n\lambda/4$, (n = 1, 3, 5 . .) are referred to as antinodes, which are the maximum amplitude positions.

Acoustic tweezing is typically performed by utilizing the USWs and many such applications can be found in the literature, such as: Jeremy Hawkes et al. deployed USW for continuous cell washing and medium exchange [57]. In [58] a technique is given to efficiently separate plasma from human whole blood which enhanced agglutination assays. Petersson et al. utilized acoustic forces in a standing wave field to discriminate lipid particles from erythrocytes in whole blood [59]. Another research group reported the retention of mammalian cells in cell culture fermentations using acoustic resonators [60]. Although the utilization of standing wave is very popular for particle handling, however, there are also examples in literature where traveling waves are deployed for micro-manipulation [61] [62] [63].

All the aforementioned examples of acoustic tweezers only allow one dimensional manipulation of the particle. Also they all deploy PZT as the transducers that have their limitations in terms of fabrication, cost, heating etc. In this thesis acoustic tweezer is designed that gives full control over particle handling by allowing 2D motion. Also CMUTs are deployed for transduction mechanism that increases the overall efficiency of the device, allows longer holding time, are easier to fabricate and are very conveniently incorporated with the microfluidic channel.

3.2.1   Primary Acoustic Radiation Forces

When an acoustic standing wave is generated in a microfluidic channel, then the particles suspended in the medium will experience a gradient force along

or against the acoustic pressure gradient which will depend on the mechanical properties of the particles. This gradient force is called the primary acoustic radiation force (PAR). This force is basically the result of the interaction between the particle and the waves and it depends on the mismatch between acoustic properties of the particles and the medium.

Acoustic radiation force was initially calculated by King [64] on an incompressible sphere in a plane standing wave in 1934. This was later extended by Yosioka and Kawasima by calculating the forces on compressible spheres in 1955 [65]. The expression was later generalized by Gorkov in 1965, who expressed the time averaged PAR force F, as a gradient of potential [66].

$$< F >= -\nabla U \tag{3.3}$$

where U is the acoustic force potential and is given by the following equation:

$$U = V[\frac{f_1}{2\rho_m c_m^2} < p^2 > -\frac{3f_2\rho_m}{4} < |v|^2 >] \tag{3.4}$$

p is the pressure field and v is the velocity field that surrounds the immersed particle. V is its volume and ρ_m and c_m are the density and sonic velocity of the medium. f_1 and f_2 are the compressibility factor and density factor. They are given as [67]:

$$f_1 = 1 - \frac{1}{\gamma\beta^2} \tag{3.5}$$

$$f_2 = \frac{2\gamma - 2}{2\gamma + 1} \tag{3.6}$$

Where γ is the ratio of sonic velocity of the particle to sonic velocity of the medium. And β is the ratio of density of the particle to density of the medium.

$$\gamma = \frac{c_p}{c_m} \tag{3.7}$$

$$\beta = \frac{\rho_p}{\rho_m} \tag{3.8}$$

19

At the resonant frequency, a strong one dimensional coupling is observed. Therefore assuming that at resonant frequency a standing wave is generated at the axial direction and that the wavelength at that frequency is much larger as compared to the particle radius, then the axial component of the primary radiation force is given as follows [67]:

$$F_{axial} = 4\pi E k \varphi \sin(2kz).R^3 \qquad (3.9)$$

φ is the acoustic contrast factor which is given as [67]:

$$\varphi = \frac{5\gamma - 2}{2\gamma + 1} - \frac{1}{\gamma \beta^2} \qquad (3.10)$$

E is the acoustic energy density which is given by the following equation:

$$E = \frac{p_a}{4\rho_m c_m^2} \qquad (3.11)$$

According to the Equation (3.9), the force increases with the radius of the particle, and therefore this imposes limit on the size of particles that can be trapped using this method. However, the force is also dependent on the resonant frequency, and working with microfluidics the small chambers lead to resonance at high frequencies. Therefore the smaller particles can be trapped by adjusting the resonant frequencies and the fluid channel lengths.

Acoustic contrast factor is another major factor that influences PAR. It determines whether the particle will be driven towards the pressure node or antinode. A solid particle, that has higher density as compared to the fluid medium, results in a positive contrast factor and that particle moves towards the pressure node. On the other hand, particles having high density and compressibility lead to a negative contrast factor and such particles are driven towards the antinode. In most of the applications, the pressure minimum is mostly at the center whereas the pressure maximum is created at the boundaries. Hence the contrast factor determines whether the particle will be trapped towards the center or at the edges of the boundary. Acoustic contrast factors of some particles is given in Table 3.1.

It has been shown by [68] that large velocity gradients give rise to a significant lateral component of the radiation force. Lateral component of the radiation force
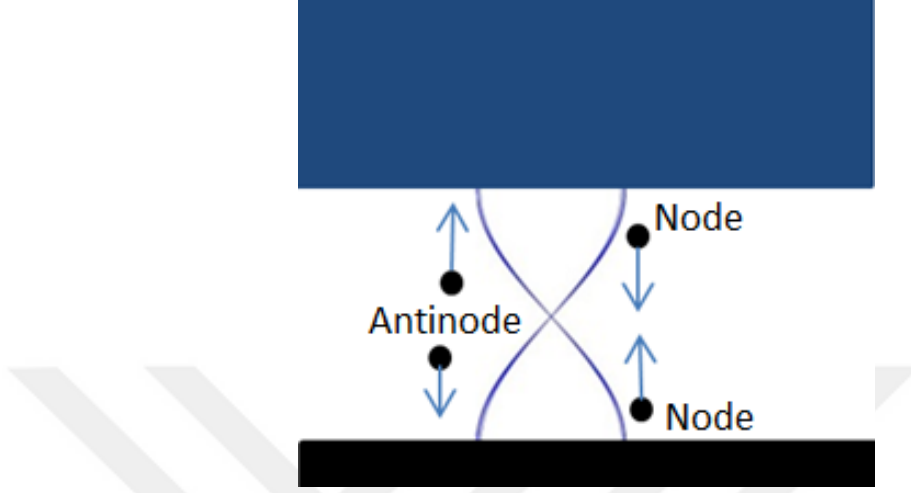
Figure 3.1: Primary axial force draws the particles towards the node or antinode depending on the acoustic contrast factor ϕ.

Particle Type	Density	Compressibility	Acoustophoretic Contrast Factor
	kg/m^3	$10^{-10}Pa^{-1}$	ϕ
Polystyrene Particle	1050	2.49	+0.165
Silica Particle	2200	0.27	+0.536
RBCs	1099	3.31	+0.12
WBCs	1019	3.995	+0.044
Colon Cancer Cell	1077	4.04	+0.06
Polyvinly air filled Microbubbles	429.6	819.67	-60.7

Table 3.1: Properties of different materials

will trap particles above the center of active elements. Although it is much smaller than the axial force, yet it is required to agglomerate particles in the trapping site and to counteract the fluid drag force. An estimate of lateral trapping force on the particles is obtained from the Stokes law which is valid because the Reynolds number of the flow is 2 x 10^{-4}.

$$F_L = 6\pi\mu c_p.R \tag{3.12}$$

Where μ is the viscosity of water.

3.2.2 Secondary Acoustic Radiation Forces

When the particles agglomerate and interact with each other then this gives rise to the secondary acoustic radiation force. Secondary forces influence the motion of the particles when the separation between them decreases and they come very close to each other. It is given by [69] as:

$$F_s = 4\pi a^6 \left(\frac{(\rho_p - \rho_m)^2 (3cos^2\theta - 1)}{6\rho_m d^4} v^2(z) - \frac{\omega^2 \rho_m (\beta_p - \beta_m)}{9d^2} p_a^2(z) \right) \tag{3.13}$$

Where d is the distance between the particles from the centers and θ is the angle between the particles and the propagation direction of the incident sound wave. θ determines whether the force will be attractive or repulsive. The influence of the SAR force, however, is very weak and becomes only important at very short distances between particles.

3.3 Microfluidic Acoustic Resonators

The typical structure of an acoustic resonator for particle handling comprises of a microfluidic channel coupled with a transducer array and a reflector on top. This is also commonly known as layered resonators. Active transducer elements generate a sound wave that reflects off the glass and creates an ultrasound standing wave within the fluid chamber, where the particles under observation are suspended.

A half wavelength resonator was developed as it brings the system fluidics into a mode of low Reynolds numbers and hence a laminar fow domain which can be easily integrated with the microfluidic channels [70] [71]. Half-wave devices are those resonators in which the fluid channel is approximately half wavelength in thickness. As described above, the acoustic radiation force is directly proportional to the resonant frequency, therefore in half wavelength resonators, the reduced dimensions lead to higher frequencies. The high frequency therefore results in higher forces causing efficient particle handling.

In order to develop a system with high Q-value, the material selection is criti-
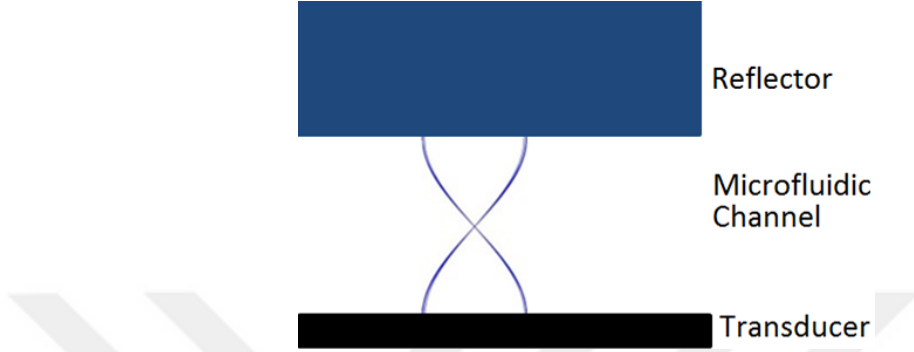

Figure 3.2: Layered acoustic resonator schematics

cal in layered resonators. In the previous designs, the selection of matching and backing layer was very critical to efficiently couple the acoustic energy into fluid medium. In this case CMUTs are used for transduction mechanism which, there-fore, simplify the design.

The purpose of reflector layer is to reflect energy back into the device, and thus maintain strong resonant operation. Glass was chosen as the reflector as it is chemically inert and hence is advantageous during the processes of microfabrica-tion. It has higher acoustic impedance as compared to water and for such systems resonance occurs across the thickness of the channel, with a pressure minimum close to the channel center. This is also useful to focus particles away from the glass walls. The transparency of the material allows observing the particle be-havior under a microscope. The materials used for the design and FEM modeling are given in Table 3.2.

Layer	Material	Density kg/m^3	Thickness μ	Sonic Velocity m/s
Fluid	Water	1000	300	1500
Reflector	Glass	2500	300	5640
Particle	Polystyrene	1055	Diameter 10	1958

Table 3.2: Model Dimensions and Layer Properties

Chapter 4

Finite Element Modeling and Analysis

Finite element methods (FEM) are used to analyze the operation of a half wavelength planar resonator. FEM is one of the most common methods used for numerical predictions and for solving several complex engineering problems. As compared to the equivalent circuit models of CMUTs, FEM gives more accurate results, as the former is based on some basic assumptions.

In all the simulations, the commercially available finite element software (ANSYS16.1) was used. The software enables a comprehensive analysis of acoustic waves in fluid medium and provides a platform to optimize the device parameters. The software also provide a fluid structure interaction, where the fluid elements are coupled to the structural elements.

In this chapter, a detailed description of the finite element modeling is given along with the simulation analysis and results.

4.1 Modeling

In order to get accurate results, the basic step is to correctly model the design. We have drawn a 3D model of the layered resonator. The first step, is to model the transducer array.

SOLID45 elements are used to model the vibrating structure. Each SOLID45 element is defined by eight nodes with each node having three degrees of freedom, i-e translations in the nodal x, y, and z directions. The elements have sufficient characteristics required to model the CMUT membrane, such as plasticity, creep, swelling, stress stiffening, large deflection, and large strain capabilities.

Four types of acoustic elements are available in ANSYS that are based on pressure formulation, which are FLUID29, FLUID30, FLUID220, and FLUID221. Where the former two are for 2D and 3D linear elements respectively and the latter two for 2D and 3D quadratic elements, respectively. We used Fluid30 to model the immersion medium which is defined by 8 nodes with each node having one pressure degree of freedom, and three translational DOFs along the x, y, and z axes. The reflector surface is also modeled with the same fluid elements.

It is mandatory to explicitly define the surface of the structure which is in contact with the fluid by using fluid structure interface flags. Fluid130 is used for simulating a 3D infinite boundary which absorbs outgoing pressure waves with little reflection into the fluid. Fluid130 are defined by four nodes, each having only pressure degree of freedom and they connect to Fluid30 elements.

For a mesh dependent study, a mesh of $\lambda/30$ was generated, where λ is the wavelength of sound wave in each material. Material properties of silicon, borosilicate glass and water as the fluid medium were assigned to the model. The assigned material properties and layer dimensions are given in the following table.

Layer	Material	Density kg/m^3	Thickness μ	Sonic Velocity m/s
Fluid	Water	1000	300	1500
Reflector	Glass	2500	300	5640
Particle	Polystyrene	1055	Diameter 10	1958

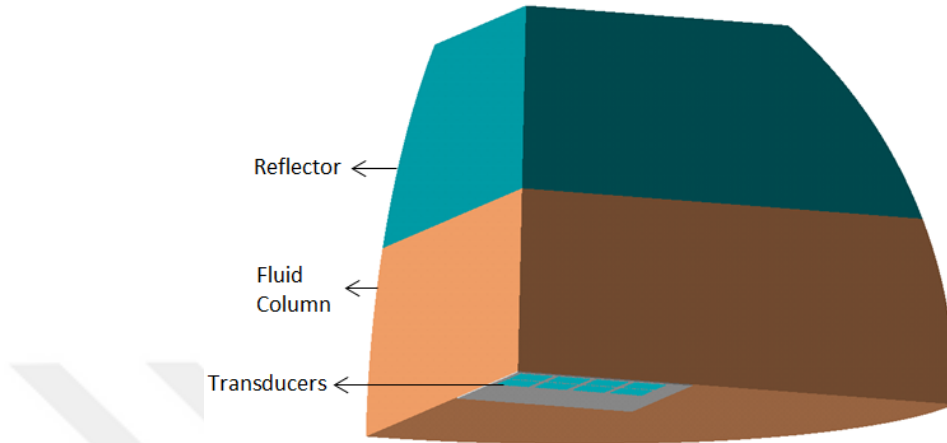Table 4.1: Model Dimensions and Layer Properties

Figure 4.1: 3D model drawn in ANSYS. The figure shows a layered resonator with transducer elements.

The electrodes were modeled using TRANS126 elements which represent a transducer element while also allowing energy storage. The element has up to two degrees of freedom i-e translation in the nodal x, y, or z direction and electric potential. The top electrode is created by taking the surface nodes of the membrane and the lower nodes are created with the TRANS126 elements which are joined to the upper nodes through a gap d. Two transducer elements comprising of 4x4 square CMUT cells with 2-μm thick membranes, 50-μm side lengths were modeled to generate pressure gradient in the fluid column. The separation between the cells was kept as 5-μm. The advantage of using square membranes is that they allow greater fill factor and hence results in an increased pressure generated in the fluid medium.

4.1.1 Boundary Conditions

The accuracy of the model depends highly on the applied boundary conditions. To save computational cost and time, we drew a 3D model and applied symmetric boundary conditions along the horizontal and vertical axis.
The boundaries of the vibrating cells are fixed, and therefore zero displacement constraints were applied to them. The bottom electrodes were also rigidly placed and therefore their movements were also restricted in the x, y and z directions.

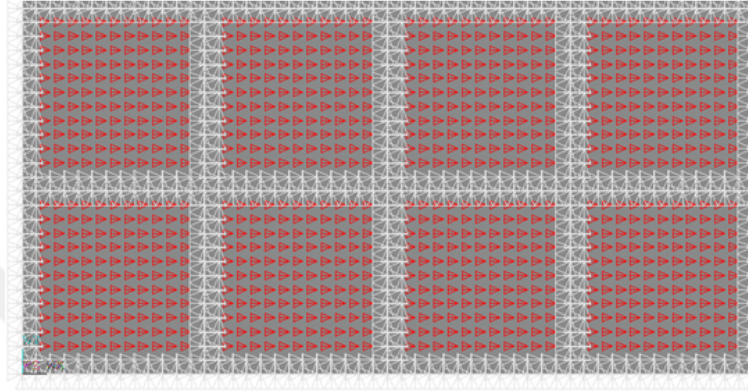The boundary conditions applied are also given in the following figure:

Figure 4.2: Applied boundary conditions. The red symbol depicts the voltage loads applied to the transducer elements. The white symbols represent the displacement constraints. The model is symmetric along the horizontal and vertical directions.

4.2 Static Structural Analysis

A static structural analysis is performed on the model that determines the displacements, stresses, strains, and forces in structures caused by the applied loads. Voltage loads were applied to the TRANS126 elements. Collapse voltage was found in this step by increasing the applied voltage in a loop until the devices started to collapse. The collapse voltage was found to be 86-V the devices were then later biased with 64-V DC in rest of the simulations. The applied voltages are high enough to generate enough pressure field required for trapping the particles while still less than the collapse voltage.

This step laid the foundation of the harmonic analysis, which is described in the next section.

4.3   Harmonic Analysis

Harmonic analyses are used to determine the steady-state response of a linear structure to harmonically varying loads. The sinusoidally varying voltage loads therefore act like the AC load. Pre-stress effects are turned on to include residual stress of the membrane. This step is critical in finding the resonant frequencies of the devices and also to understand the fields generated due to the applied frequency. At resonance the membrane exhibits maximum center deflection. The
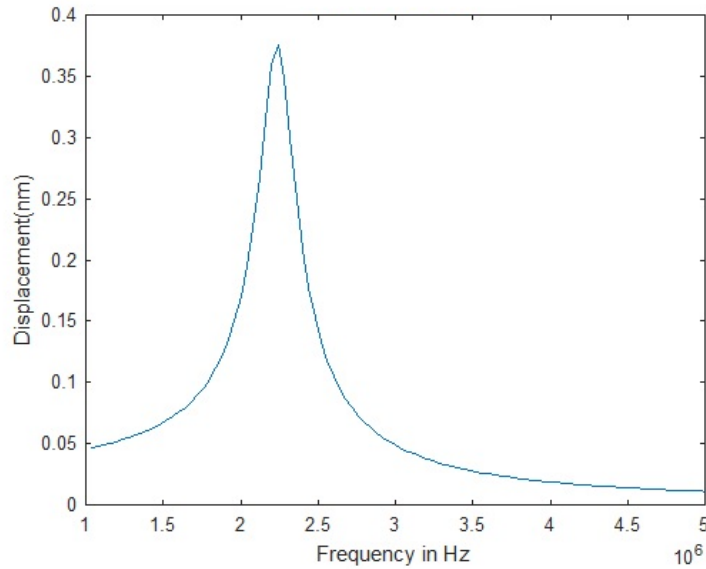
Figure 4.3: Center deflection of a single membrane.

resonant frequency of a single cell with the same design parameters was found to be 2.34Mhz. The devices were driven with $24V_{p-p}$.

Pressure field distribution and velocity of the particles in fluid medium were also found during the harmonic analysis. By activating adjacent 4 (2x2) transducer elements, a pressure node was created at the center of the fluid channel which shows trapping site of the particle.
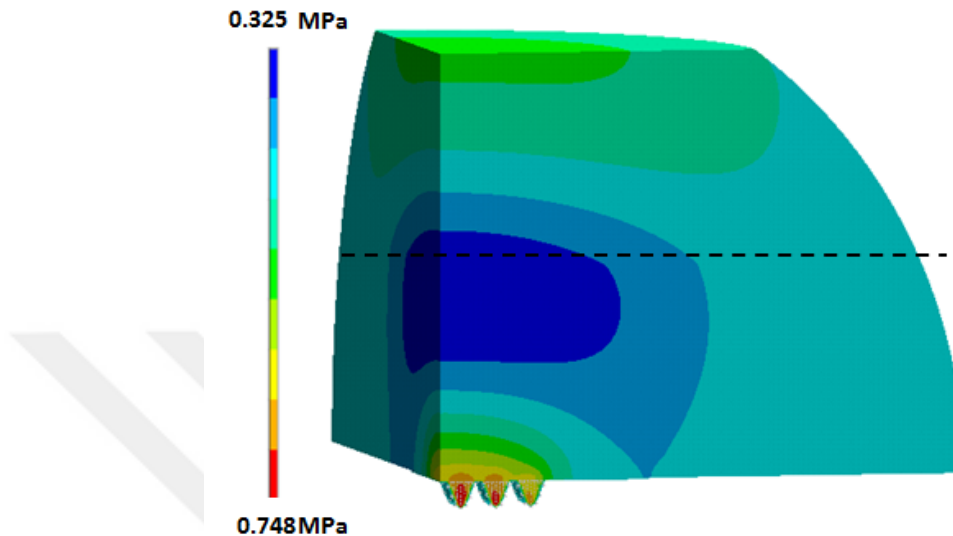
Figure 4.4: Pressure field in the resonator. The dashed line shows the boundary between the glass and the fluid column.

4.4   Row column Addressed CMUT Arrays

To understand the response of the devices in row column addressed CMUT arrays were modeled as well. In the RC approach, the column electrodes are biased with DC voltage whereas voltage pulses are applied to the rows. The general idea of RC array is illustrated in the Figure 4.4.

This scheme, therefore, does not give an electronic control over one single element. To understand the effect of inactive elements, we simulated a 6x6 CMUT array with each element containing 3x3 CMUT cells and performed a transient analysis illustrated in Figure 4.4.

4.4.1   Transient Analysis

Transient analysis is used to determine the dynamic response of a structure under time-dependent loads. This analysis gives a better insight to operation of the devices. A transient analysis was performed for a time period of 400-ns to observe

29
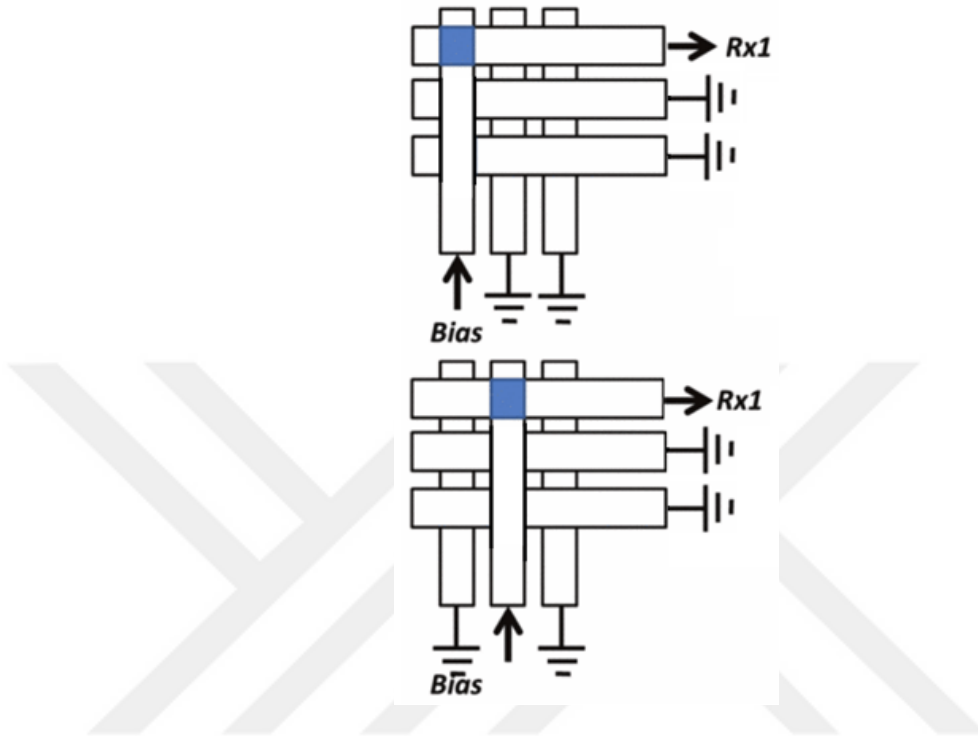
Figure 4.5: Illustration of RC array idea.

pressure field extending in the lateral and axial directions. The pressure field generated by the inactive elements is very low and therefore does not contribute in particle handling Figure 4.5.

4.5 Results and Discussion

Finite element analysis gives a good approximation of the device behavior and the trapping site. The force on a 10-μm polystyrene was calculated using Equation 3.9 which was found to be 132 pN. The lateral force was found to be 3.31 pN from Equation 3.12. Plotting the acoustic force potential, U, is another convenient way of visualizing the acoustic forces. Particles will tend to move towards regions where U is minimum. This also corresponds to the pressure minimum formed at the center of the channel due to half wavelength design.
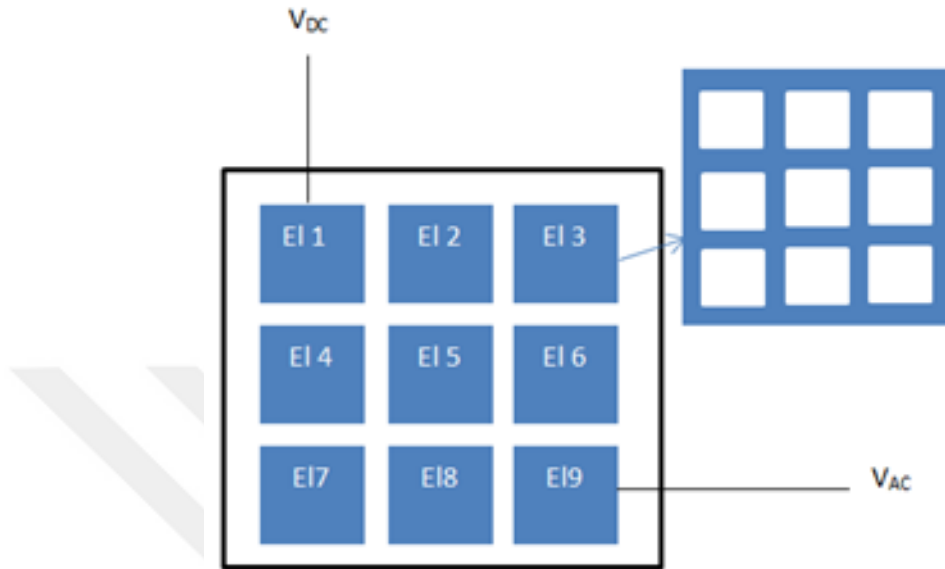
Figure 4.6: Illustration of the simulated design.

The finite element analysis results clearly demonstrate that the acoustic potential minimum is generated at the center of the microfluidic channel. Using the same parameters, masks were created using KLayout for fabricating the RC arrays. The fabrication process is discussed in the following chapter.
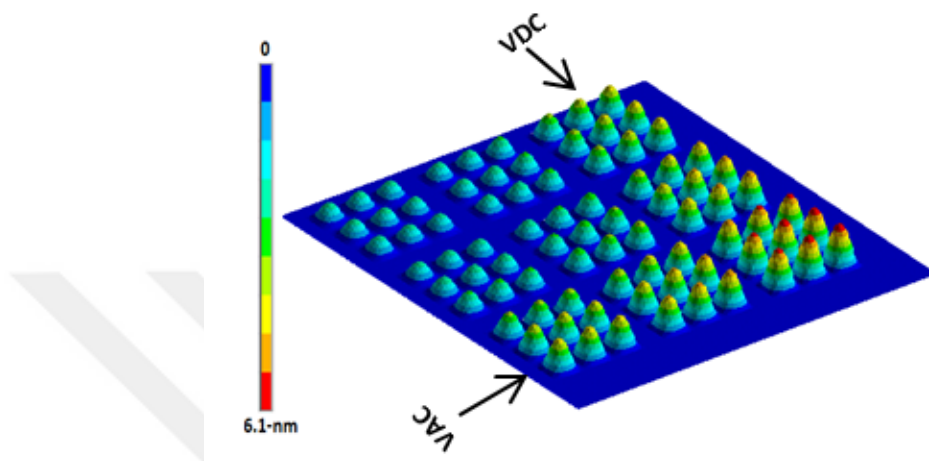
Figure 4.7: Deflection of membranes when the membranes in the column are biased with DC and AC voltage is applied to the rows.
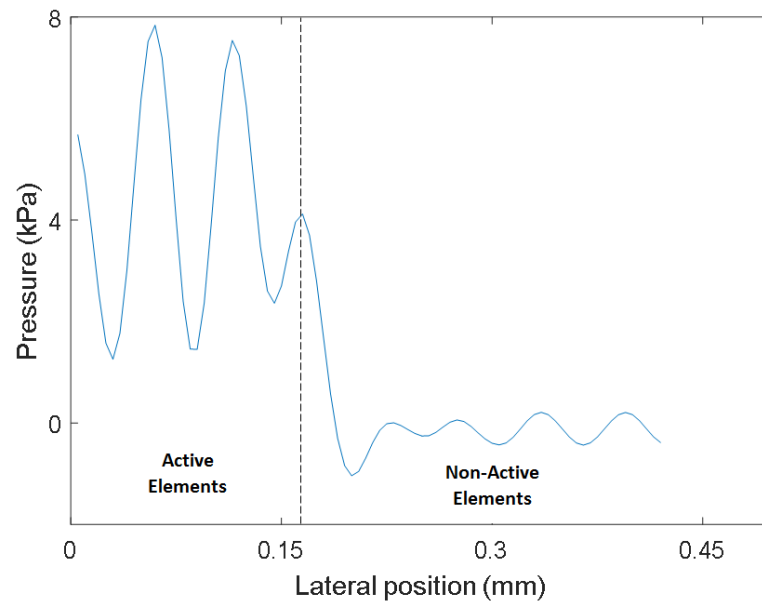
Figure 4.8: Lateral pressure distribution along the center line of fluid channel for 2x2 active elements
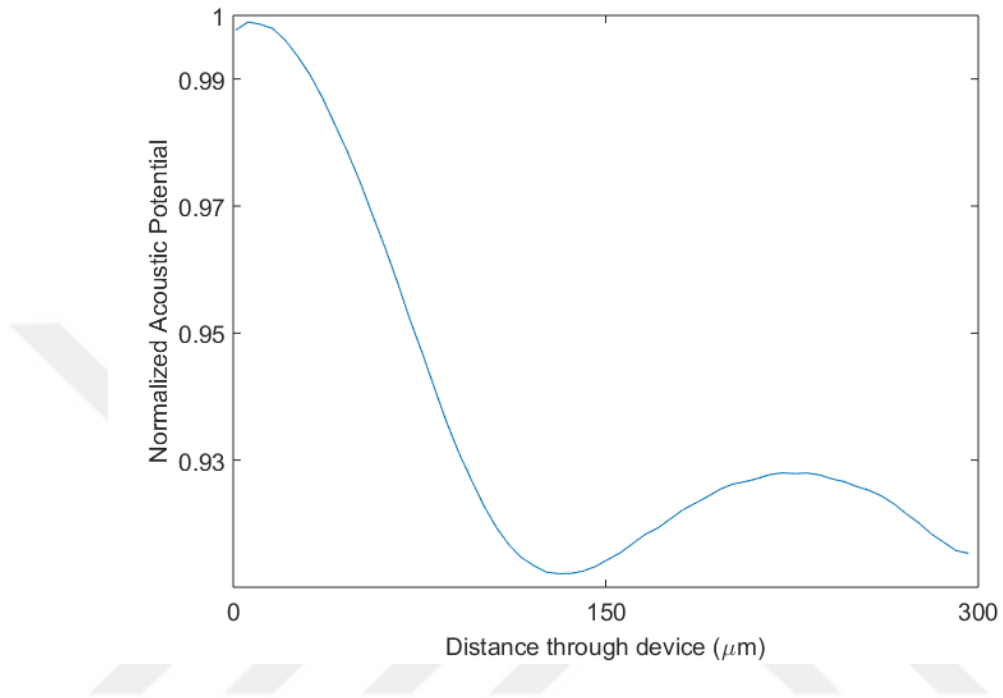
Figure 4.9: Plot of acoustic potential along the thickness of the microfluidic channel
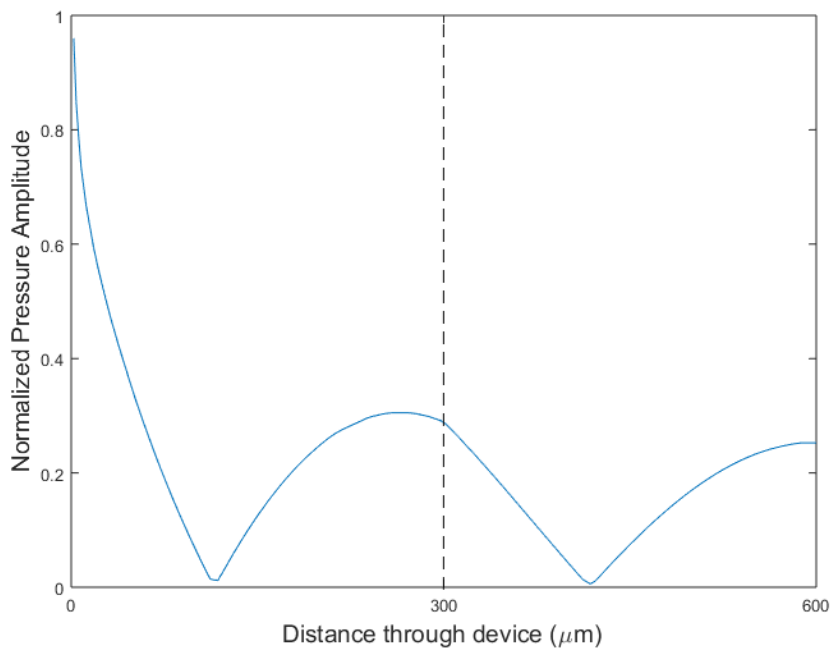
Figure 4.10: Normalized pressure distribution corresponding to the pressure minima

Chapter 5

Fabrication of RC Arrays

In order to allow two dimensional manipulation of particles in the microfluidic channel a row column-addressed CMUT arrays were developed that serve as a basis of the microfluidic platform.

The fabrication of 2D CMUT array holds some challenges; as they not only difficult to fabricate but also the integration with the front end circuit is a serious issue. If there are N number of elements then the 2D array leads to NxN number of channels making the fabrication of large 2D array cost prohibitive. In some of the earlier attempts, the contacts are brought to the backside of the wafer by deploying through-silicon via (TSV) interconnects [72]. In this approach polysilicon is used as bottom electrode and the via material causes roughness in the cavities that degrades the performance of the devices. Many techniques have been developed that use through-wafer electrical interconnect which is compatible with both the surface micromachined and the SOI wafer-bonded CMUTs fabrication methods [73] [74] [72]. All these techniques have resulted in an increased process complexity.

An attractive alternative is the row column addressed arrays, where the electrodes are connected such that each row and each column of the array is individually addressable.

In early RC CMUT arrays, rows and columns of the array acted like one large element and hence lacked single element actuation, which leads to edge effects in imaging applications [75] [76]. This issue has been addressed by using top orthogonal to bottom electrode (TOBE) arrays [77] [78], where a single element has been addressed by biasing column and exciting the corresponding row with pulse. The fabrication of TOBE arrays is done on SOI wafers that incur parasitic effects due to silicon substrate. The issue has also been addressed by integrating apodization in the transducer array [79]. They fabricated CMUT devices by bonding two SOI wafers. This technique is comparatively simpler but the rows of these devices get coupled with the bottom SOI wafer and hence degrades the performance of the devices.

In this work, a fabrication technique proposed by [31] was adapted. This approach offers many advantages such as simpler fabrication, increased fill factor and effective membrane uniformity. Also, the use of borosilicate glass as the substrate prevents electrical coupling between the bottom electrodes and the substrate [80].

5.1   Cavities and Bottom Electrode

The fabrication process is started by thoroughly cleaning the borosilicate wafer in Piranha solution, which is the mixture of 70% sulfuric acid (H_2SO_4) and 30% hydrogen peroxide (H_2O_2). This is important as the impurities could lead to issues during the bonding step.

Photolithography techniques were employed for producing high precision patterning on substrates and are one of the most important steps in micro-fabrication. The general procedure of photolithography begins with a substrate, which is then coated with photoresist. Photoresist is a material that changes solubility when exposed to light, the solubility of positive photoresist increases in light on the contrary the solubility of negative photoresists increases in the shadow. This substrate is then exposed to light through a transparent mask with desired patterns. The exposed substrate is then developed using different solvents to leave a permanent pattern on the substrate.

In our fabrication technique the first photolithography step was used to pattern

the shape of the cavities on the substrate using a negative photoresists. The patterned wafer was hard baked at 125°C to improve adhesion between the wafer and the photoresist and makes it a better mask for etching.

Etching is also one of the main processes in micro-fabrication as it involves removing materials in the desired areas by physical or chemical means. After a pattern is established on the substrate using photolithography then to shape the geometry of microcomponents etching techniques are used. The two main types of etching are dry etching and wet etching. Where in the former case the desired materials are removed using gaseous etchants by employing either plasma, ion milling or reactive ion etching (R—E). Where as the latter technique involves removing materials with diluted chemicals to dissolve substrate.

In order to create cavities we used wet etching in 10:1 buffered oxide etch (BOE) solution. The wet etching was preferred as it results in less surface roughness in the cavities and more uniform etching. 350-nm deep cavities were created through this process and 130-nm gold and 20-nm chromium adhesion layers were deposited to obtain 150-nm bottom electrode Figure 5.1 (c).

5.2   Wafer Bonding

As already mentioned previously an insulation layer of silicon nitride is incorporated between the top and bottom electrode to avoid any electrical shorting if the two electrodes come in contact with each other in case the CMUT cell collapses. To form the insulation layer a silicon nitride layer of 200-nm thickness was deposited on top of the device layer of the SOI wafer by plasma enhanced chemical vapor deposition (PECVD). Chemical vapor deposition (CVD) is a technique used in microfabrication processes that require the deposition of thin films. In this technique gases with diffused reactants are flowed over a hot substrate surface and this interaction results in the deposition of the desired film over the substrate surface. PECVD is a type of chemical vapor deposition that uses radio frequency (RF) plasma to transfer energy into the reactant gases and hence allowing the substrate to remain at a lower temperature as compared to the other techniques

of CVD.

Now that the two wafers were ready, the glass wafer and the SOI wafers were again cleaned using solvents and Pirhana solution, respectively. Borosilicate glass and the silicon nitride surfaces were anodically bonded together at 350ºC under 2.5-kN down force and 700-V bias voltage in vacuum, Figure 5.1 (e). The handle layer was then ground to 100-μm and the rest was removed by using heated tetramethyammonium hydroxide (TMAH) solution at 85ºC. The membrane was released after removing the BOX layer by using 10:1 BOE solution.

5.3   Accessing Pads

In order to access the metal pads, silicon/silicon nitride layer on the location of pads was etched by reactive ion etching (RIE) with SF6 Figure 5.1 (f). During anodic bonding, the borosilicate substrate is exposed to high electrostatic field and it results in outgassing [81]. This restricts the application of these devices that require vacuum-sealed cavities. Hence when the silicon/silicon nitride layers are etched on the locations of metal pads, the trapped gas also evacuates which solves the outgassing problem in the devices.

This step also separates rows and creates dicing lines that separate different arrays. The photoresist was removed by oxygen plasma. To seal the cavities a conformal PECVD silicon nitride layer was deposited, the thickness of which was chosen to be three times the cavity height for a proper sealing [8]. This layer also serves as an insulation between the transducers and the microfluidic channel.

5.4   Electrical Connections

In the previous step, the devices were completely covered by silicon nitride. Therefore to create electrical connections the silicon nitride layer on the pads' locations required to be removed. This was done by using the final mask, which removed silicon nitride by reactive ion etching at locations where contact pads would

be made. After removing the nitride layer, 180-nm gold and 20-nm chromium was deposited to ensure a good electrical contact and to improve the conductivity of the row electrodes, Figure 5.1 (h). Figure 5.2 shows the fabricated RC array and the close-up view shows the array elements in Figure 5.3.
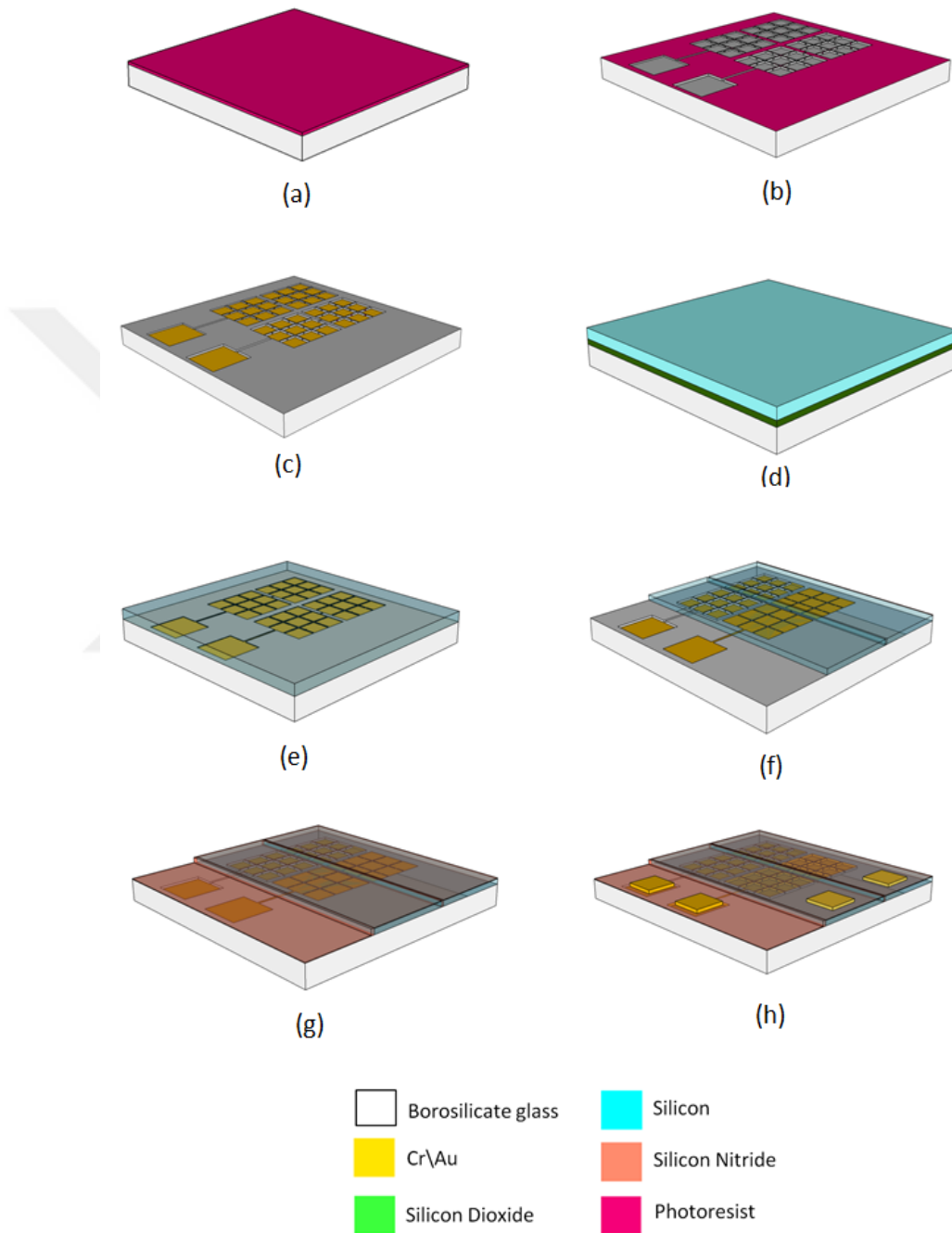
Figure 5.1: Fabrication flow: (a) Photoresist coated on top of the borosilicate (b) Cavities through BOE etch. (c) Metal deposition and lift-off. (d) Anodic bonding. (e) Handle and Box Removal. (f) Silicon etching for addressing rows. (g) Silicon nitride deposition. (h) Reaching pads through silicon nitride etching followed by metal deposition and lift-off.
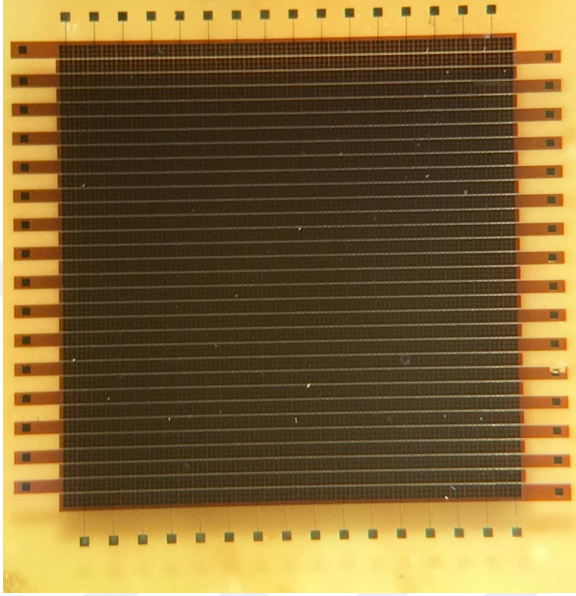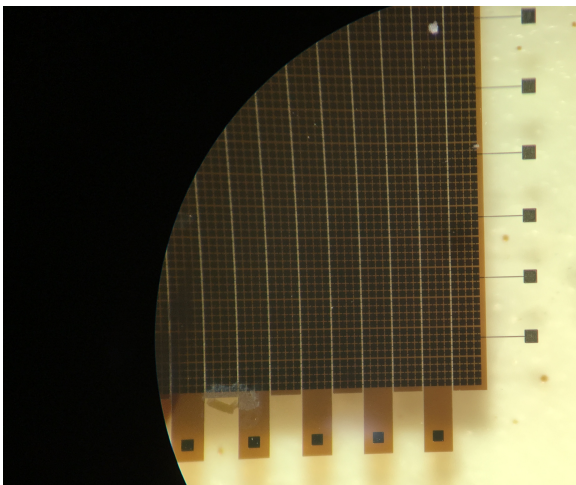
Figure 5.2: Fabricated RC CMUT arrays

Figure 5.3: Zoomed view to show the array elements

Chapter 6

Discussion and Future Work

In this work, a micromanipulation platform was designed that allowed two dimensional manipulation of particles without requiring any invasive contact, tagging, or biochemical labeling. A 2D row column addressed CMUT array has been integrated into a multilayer planar ultrasonic resonator to agglomerate particles along the center of the channel and then move them in horizontal or vertical directions by activating the elements of the array.

In half wavelength resonators the suspended micro-particles are driven towards the center of the channel due to the potential energy density minimum. The simulation results were in accordance with the theory and showed the trapping positions. The device presented in the thesis consists of a 300-μm thick microfluidic channel, which corresponds to 2.5MHz operating frequency, incorporated with the transducer array on one side and 300-μm thick glass as a reflector. The two active elements generated an acoustic force that could be used for micro manipulation of particles. Simulations confirm that forces on particles, such as 10-μm polystyrene beads, are dominated by the pressure gradient in the field, the gradient in the acoustic particle velocity field is sufficient for lateral manipulation. A row column addressed CMUT arrays were fabricated using wafer bonding techniques. This novel fabrication method can be easily integrated with an electronic circuit and also incorporates microfluidic channel very conveniently. The use of an insulator as a substrate considerably reduces the parasitic capacitance and

thus improves sensitivity of the devices.

The RC arrays can be employed in a number of ways. For example The decrease in the cable count makes them a strong candidate for 3D imaging applications. The current RC arrays suffer from parasitic capacitance issue and hence degrade the quality of imaging. Therefore, we believe that these arrays could also be extended for imaging applications.

Bibliography

[1] T. L. Szabo, *Diagnostic ultrasound imaging: inside out.* Academic Press, 2004.

[2] M. Lukacs, J. Yin, G. Pang, R. C. Garcia, E. Cherin, R. Williams, J. Mehi, and F. S. Foster, "Performance and characterization of new micromachined high-frequency linear arrays," *IEEE transactions on ultrasonics, ferroelectrics, and frequency control*, vol. 53, no. 10, 2006.

[3] R. S. Cobbold, *Foundations of biomedical ultrasound.* Oxford University Press, 2006.

[4] A. Arnau *et al.*, *Piezoelectric transducers and applications*, vol. 2004. Springer, 2004.

[5] P. Augustsson, J. Malm, and S. Ekström, "Acoustophoretic microfluidic chip for sequential elution of surface bound molecules from beads or cells," *Biomicrofluidics*, vol. 6, no. 3, p. 034115, 2012.

[6] O. Oralkan, A. S. Ergun, C.-H. Cheng, J. A. Johnson, M. Karaman, T. H. Lee, and B. T. Khuri-Yakub, "Volumetric imaging using 2d capacitive micromachined ultrasonic transducer arrays (cmuts): Initial results," in *Ultrasonics Symposium, 2002. Proceedings. 2002 IEEE*, vol. 2, pp. 1083–1086, IEEE, 2002.

[7] B. Bayram, E. Hæggstrom, G. G. Yaralioglu, and B. T. Khuri-Yakub, "A new regime for operating capacitive micromachined ultrasonic transducers," *ieee transactions on ultrasonics, ferroelectrics, and frequency control*, vol. 50, no. 9, pp. 1184–1190, 2003.

[8] M. I. Haller and B. T. Khuri-Yakub, "A surface micromachined electrostatic ultrasonic air transducer," *IEEE Transactions on Ultrasonics, Ferroelectrics, and Frequency Control*, vol. 43, no. 1, pp. 1–6, 1996.

[9] M. Haller and B. Khuri-Yakub, "Micromachined 1–3 composites for ultrasonic air transducers," *Review of scientific instruments*, vol. 65, no. 6, pp. 2095–2098, 1994.

[10] O. Oralkan, S. T. Hansen, B. Bayram, G. G. Yaralioglu, A. S. Ergun, and B. T. Khuri-Yakub, "High-frequency cmut arrays for high-resolution medical imaging," in *Ultrasonics Symposium, 2004 IEEE*, vol. 1, pp. 399–402, IEEE, 2004.

[11] D. M. Mills, "Medical imaging with capacitive micromachined ultrasound transducer (cmut) arrays," in *Ultrasonics Symposium, 2004 IEEE*, vol. 1, pp. 384–390, IEEE, 2004.

[12] C. Daft, P. Wagner, B. Bymaster, S. Panda, K. Patel, and I. Ladabaum, "cmuts and electronics for 2d and 3d imaging: monolithic integration, in-handle chip sets and system implications," in *Ultrasonics Symposium, 2005 IEEE*, vol. 1, pp. 463–474, IEEE, 2005.

[13] M. Wang, J. Chen, X. Cheng, J.-C. Cheng, and P.-C. Li, "Design and test of a monolithic ultrasound-image-guided hifu device using annular cmut rings," in *Ultrasonics Symposium, 2008. IUS 2008. IEEE*, pp. 459–462, IEEE, 2008.

[14] S. H. Wong, M. Kupnik, R. D. Watkins, K. Butts-Pauly, and B. T. Khuri-Yakub, "Capacitive micromachined ultrasonic transducers for therapeutic ultrasound applications," *IEEE transactions on Biomedical Engineering*, vol. 57, no. 1, pp. 114–123, 2010.

[15] P. Cristman, O. Oralkan, X. Zhuang, T.-J. Ma, S. Vaithilingam, T. Carver, I. Wygant, and B. Khuri-Yakub, "A 2d cmut hydrophone array: Characterization results," in *Ultrasonics Symposium (IUS), 2009 IEEE International*, pp. 992–995, IEEE, 2009.

[16] H. Jagannathan, G. G. Yaralioglu, A. S. Ergun, F. Degertekin, and B. Khuri-Yakub, "Micro-fluidic channels with integrated ultrasonic transducers," in *Ultrasonics Symposium, 2001 IEEE*, vol. 2, pp. 859–862, IEEE, 2001.

[17] S. Vaithilingam, T.-J. Ma, Y. Furukawa, I. O. Wygant, X. Zhuang, A. De La Zerda, O. Oralkan, A. Kamaya, R. B. Jeffrey, B. T. Khuri-yakub, *et al.*, "Three-dimensional photoacoustic imaging using a two-dimensional cmut array," *IEEE transactions on ultrasonics, ferroelectrics, and frequency control*, vol. 56, no. 11, pp. 2411–2419, 2009.

[18] S. W. Lani, M. Wasequr Rashid, J. Hasler, K. G. Sabra, and F. Levent Degertekin, "Capacitive micromachined ultrasonic transducer arrays as tunable acoustic metamaterials," *Applied physics letters*, vol. 104, no. 5, p. 051914, 2014.

[19] S. Hansen, N. Irani, F. L. Degertekin, I. Ladabaum, and B. Khuri-Yakub, "Defect imaging by micromachined ultrasonic air transducers," in *Ultrasonics Symposium, 1998. Proceedings., 1998 IEEE*, vol. 2, pp. 1003–1006, IEEE, 1998.

[20] X. Wang, Y. Fan, W.-C. Tian, H.-J. Kwon, S. Kennerly, G. Claydon, and A. May, "Development of air-coupled ultrasound transducers for nondestructive evaluation," in *Micro Electro Mechanical Systems, 2008. MEMS 2008. IEEE 21st International Conference on*, pp. 932–935, IEEE, 2008.

[21] H. Lee, K. Park, P. Cristman, O. Oralkan, M. Kupnik, and B. Khuri-Yakub, "A low-noise oscillator based on a multi-membrane cmut for high sensitivity resonant chemical sensors," in *Micro Electro Mechanical Systems, 2009. MEMS 2009. IEEE 22nd International Conference on*, pp. 761–764, IEEE, 2009.

[22] K. K. Park, H. Lee, M. Kupnik, Ö. Oralkan, J.-P. Ramseyer, H. P. Lang, M. Hegner, C. Gerber, and B. T. Khuri-Yakub, "Capacitive micromachined ultrasonic transducer (cmut) as a chemical sensor for dmmp detection," *Sensors and Actuators B: Chemical*, vol. 160, no. 1, pp. 1120–1127, 2011.

[23] O. Oralkan, A. S. Ergun, J. A. Johnson, M. Karaman, U. Demirci, K. Kaviani, T. H. Lee, and B. T. Khuri-Yakub, "Capacitive micromachined ultrasonic transducers: Next-generation arrays for acoustic imaging?," *IEEE transactions on ultrasonics, ferroelectrics, and frequency control*, vol. 49, no. 11, pp. 1596–1610, 2002.

[24] A. Bozkurt, F. Degertekin, A. Atalar, and B. Khuri-Yakub, "Analytic modeling of loss and cross-coupling in capacitive micromachined ultrasonic transducers," in *Ultrasonics Symposium, 1998. Proceedings., 1998 IEEE*, vol. 2, pp. 1025–1028, IEEE, 1998.

[25] B. Bayram, G. G. Yaralioglu, A. S. Ergun, and B. Khuri-Yakub, "Influence of the electrode size and location on the performance of a cmut [us transducer]," in *Ultrasonics Symposium, 2001 IEEE*, vol. 2, pp. 949–952, IEEE, 2001.

[26] Y. Roh and B. T. Khuri-Yakub, "Finite element analysis of underwater capacitor micromachined ultrasonic transducers," *IEEE transactions on ultrasonics, ferroelectrics, and frequency control*, vol. 49, no. 3, pp. 293–298, 2002.

[27] I. O. Wygant, M. Kupnik, J. C. Windsor, W. M. Wright, M. S. Wochner, G. G. Yaralioglu, M. F. Hamilton, and B. T. Khuri-Yakub, "50 khz capacitive micromachined ultrasonic transducers for generation of highly directional sound with parametric arrays," *IEEE transactions on ultrasonics, ferroelectrics, and frequency control*, vol. 56, no. 1, pp. 193–203, 2009.

[28] Y. Huang, A. S. Ergun, E. Haeggstrom, M. H. Badi, and B. T. Khuri-Yakub, "Fabricating capacitive micromachined ultrasonic transducers with wafer-bonding technology," *Journal of microelectromechanical systems*, vol. 12, no. 2, pp. 128–137, 2003.

[29] A. Erguri, Y. Huang, X. Zhuang, O. Oralkan, G. G. Yarahoglu, and B. T. Khuri-Yakub, "Capacitive micromachined ultrasonic transducers: Fabrication technology," *IEEE transactions on ultrasonics, ferroelectrics, and frequency control*, vol. 52, no. 12, pp. 2242–2258, 2005.

[30] N. Tas, T. Sonnenberg, H. Jansen, R. Legtenberg, and M. Elwenspoek, "Stiction in surface micromachining," *Journal of Micromechanics and Microengineering*, vol. 6, no. 4, p. 385, 1996.

[31] F. Y. Yamaner, X. Zhang, and Ö. Oralkan, "A three-mask process for fabricating vacuum-sealed capacitive micromachined ultrasonic transducers using anodic bonding," *IEEE transactions on ultrasonics, ferroelectrics, and frequency control*, vol. 62, no. 5, pp. 972–982, 2015.

[32] A. Ashkin and J. M. Dziedzic, "Optical trapping and manipulation of viruses and bacteria," *Science*, vol. 235, pp. 1517–1521, 1987.

[33] F. Arai, C. Ng, H. Maruyama, A. Ichikawa, H. El-Shimy, and T. Fukuda, "On chip single-cell separation and immobilization using optical tweezers and thermosensitive hydrogel," *Lab on a Chip*, vol. 5, no. 12, pp. 1399–1403, 2005.

[34] Y. Arai, R. Yasuda, K.-i. Akashi, Y. Harada, H. Miyata, K. Kinosita, and H. Itoh, "Tying a molecular knot with optical tweezers," *Nature*, vol. 399, no. 6735, pp. 446–448, 1999.

[35] K. C. Neuman, E. H. Chadd, G. F. Liou, K. Bergman, and S. M. Block, "Characterization of photodamage to escherichia coli in optical traps," *Biophysical journal*, vol. 77, no. 5, pp. 2856–2863, 1999.

[36] A. Manz, N. Graber, and H. á. Widmer, "Miniaturized total chemical analysis systems: a novel concept for chemical sensing," *Sensors and actuators B: Chemical*, vol. 1, no. 1-6, pp. 244–248, 1990.

[37] G. P. Hatch and R. E. Stelter, "Magnetic design considerations for devices and particles used for biological high-gradient magnetic separation (hgms) systems," *Journal of Magnetism and Magnetic Materials*, vol. 225, no. 1, pp. 262–276, 2001.

[38] H. A. Pohl, "The motion and precipitation of suspensoids in divergent electric fields," *Journal of Applied Physics*, vol. 22, no. 7, pp. 869–871, 1951.

[39] A. Kundt and O. Lehmann, "Ueber longitudinale schwingungen und klang-figuren in cylindrischen flüssigkeitssäulen," *Annalen der Physik*, vol. 229, no. 9, pp. 1–12, 1874.

[40] P. R. Mayeux, "Pathobiology of lipopolysaccharide," *Journal of toxicology and environmental health*, vol. 51, no. 5, pp. 415–435, 1997.

[41] V. I. Furdui and D. J. Harrison, "Immunomagnetic t cell capture from blood for pcr analysis using microfluidic systems," *Lab on a Chip*, vol. 4, no. 6, pp. 614–618, 2004.

[42] C. W. Shields IV, C. D. Reyes, and G. P. López, "Microfluidic cell sorting: a review of the advances in the separation of cells from debulking to rare cell isolation," *Lab on a Chip*, vol. 15, no. 5, pp. 1230–1249, 2015.

[43] J. H. Kang, S. Krause, H. Tobin, A. Mammoto, M. Kanapathipillai, and D. E. Ingber, "A combined micromagnetic-microfluidic device for rapid capture and culture of rare circulating tumor cells," *Lab on a Chip*, vol. 12, no. 12, pp. 2175–2181, 2012.

[44] K. Hoshino, Y.-Y. Huang, N. Lane, M. Huebschman, J. W. Uhr, E. P. Frenkel, and X. Zhang, "Microchip-based immunomagnetic detection of circulating tumor cells," *Lab on a Chip*, vol. 11, no. 20, pp. 3449–3457, 2011.

[45] C. W. Shields IV, C. E. Livingston, B. B. Yellen, G. P. López, and D. M. Murdoch, "Magnetographic array for the capture and enumeration of single cells and cell pairs," *Biomicrofluidics*, vol. 8, no. 4, p. 041101, 2014.

[46] F. Brosseron, K. Marcus, and C. May, "Isolating peripheral lymphocytes by density gradient centrifugation and magnetic cell sorting," *Proteomic Profiling: Methods and Protocols*, pp. 33–42, 2015.

[47] K.-H. Han and A. B. Frazier, "A microfluidic system for continuous magnetophoretic separation of suspended cells using their native magnetic properties," *Proc. Nanotech*, vol. 1, pp. 187–190, 2005.

[48] T. Kimura, M. Yamato, and A. Nara, "Particle trapping and undulation of a liquid surface using a microscopically modulated magnetic field," *Langmuir*, vol. 20, no. 3, pp. 572–574, 2004.

[49] A. Winkleman, K. L. Gudiksen, D. Ryan, G. M. Whitesides, D. Greenfield, and M. Prentiss, "A magnetic trap for living cells suspended in a paramagnetic buffer," *Applied physics letters*, vol. 85, no. 12, pp. 2411–2413, 2004.

[50] M. Zborowski, P. S. Malchesky, T.-F. Jan, and G. S. Hall, "Quantitative separation of bacteria in saline solution using lanthanide er (iii) and a magnetic field," *Microbiology*, vol. 138, no. 1, pp. 63–68, 1992.

[51] H. Lee, A. Purdon, and R. Westervelt, "Manipulation of biological cells using a microelectromagnet matrix," *Applied physics letters*, vol. 85, no. 6, pp. 1063–1065, 2004.

[52] P. Sajeesh and A. K. Sen, "Particle separation and sorting in microfluidic devices: a review," *Microfluidics and nanofluidics*, vol. 17, no. 1, pp. 1–52, 2014.

[53] L. M. Barrett, A. J. Skulan, A. K. Singh, E. B. Cummings, and G. J. Fiechtner, "Dielectrophoretic manipulation of particles and cells using insulating ridges in faceted prism microchannels," *Analytical chemistry*, vol. 77, no. 21, pp. 6798–6804, 2005.

[54] E. B. Cummings and A. K. Singh, "Dielectrophoresis in microchips containing arrays of insulating posts: theoretical and experimental results," *Analytical chemistry*, vol. 75, no. 18, pp. 4724–4731, 2003.

[55] Y. Huang, S. Joo, M. Duhon, M. Heller, B. Wallace, and X. Xu, "Dielectrophoretic cell separation and gene expression profiling on microelectronic chip arrays," *Analytical chemistry*, vol. 74, no. 14, pp. 3362–3371, 2002.

[56] X. Hu, P. H. Bessette, J. Qian, C. D. Meinhart, P. S. Daugherty, and H. T. Soh, "Marker-specific sorting of rare cells using dielectrophoresis," *Proceedings of the National Academy of Sciences of the United States of America*, vol. 102, no. 44, pp. 15757–15761, 2005.

[57] J. J. Hawkes, R. W. Barber, D. R. Emerson, and W. T. Coakley, "Continuous cell washing and mixing driven by an ultrasound standing wave within a microfluidic channel," *Lab on a Chip*, vol. 4, no. 5, pp. 446–452, 2004.

[58] C. Cousins, P. Holownia, J. Hawkes, M. Limaye, C. Price, P. Keay, and W. Coakley, "Plasma preparation from whole blood using ultrasound," *Ultrasound in medicine & biology*, vol. 26, no. 5, pp. 881–888, 2000.

[59] F. Petersson, A. Nilsson, C. Holm, H. Jönsson, and T. Laurell, "Separation of lipids from blood utilizing ultrasonic standing waves in microfluidic channels," *Analyst*, vol. 129, no. 10, pp. 938–943, 2004.

[60] M. Grösch, W. Burger, B. Handl, O. Doblhoff-Dier, T. Gaida, and C. Schmatz, "Ultrasonic separation of suspended particles-part iii: Application in biotechnology," *Acta Acustica united with Acustica*, vol. 84, no. 5, pp. 815–822, 1998.

[61] S. H. Cho, C. H. Chen, F. S. Tsai, J. M. Godin, and Y.-H. Lo, "Human mammalian cell sorting using a highly integrated micro-fabricated fluorescence-activated cell sorter (μfacs)," *Lab on a Chip*, vol. 10, no. 12, pp. 1567–1573, 2010.

[62] T. Franke, S. Braunmüller, L. Schmid, A. Wixforth, and D. Weitz, "Surface acoustic wave actuated cell sorting (sawacs)," *Lab on a Chip*, vol. 10, no. 6, pp. 789–794, 2010.

[63] L. Schmid, D. A. Weitz, and T. Franke, "Sorting drops and cells with acoustics: acoustic microfluidic fluorescence-activated cell sorter," *Lab on a Chip*, vol. 14, no. 19, pp. 3710–3718, 2014.

[64] L. V. King, "On the acoustic radiation pressure on spheres," in *Proceedings of the Royal Society of London A: Mathematical, Physical and Engineering Sciences*, vol. 147, pp. 212–240, The Royal Society, 1934.

[65] K. Yosioka and Y. Kawasima, "Acoustic radiation pressure on a compressible sphere," *Acta Acustica united with Acustica*, vol. 5, no. 3, pp. 167–173, 1955.

[66] M. Settnes and H. Bruus, "Forces acting on a small particle in an acoustical field in a viscous fluid," *Physical Review E*, vol. 85, no. 1, p. 016327, 2012.

[67] R. Barnkob, P. Augustsson, T. Laurell, and H. Bruus, "Measuring the local pressure amplitude in microchannel acoustophoresis," *Lab on a Chip*, vol. 10, no. 5, pp. 563–570, 2010.

[68] A. Lenshof, M. Evander, T. Laurell, and J. Nilsson, "Acoustofluidics 5: Building microfluidic acoustic resonators," *Lab on a Chip*, vol. 12, no. 4, pp. 684–695, 2012.

[69] M. Gröschl, "Ultrasonic separation of suspended particles-part i: Fundamentals," *Acta Acustica united with Acustica*, vol. 84, no. 3, pp. 432–447, 1998.

[70] K. Yasuda, S.-i. Umemura, and K. Takeda, "Concentration and fractionation of small particles in liquid by ultrasound," *Japanese journal of applied physics*, vol. 34, no. 5S, p. 2715, 1995.

[71] D. A. Johnson and D. L. Feke, "Methodology for fractionating suspended particles using ultrasonic standing wave and divided flow fields," *Separations Technology*, vol. 5, no. 4, pp. 251–258, 1995.

[72] C. H. Cheng, E. M. Chow, X. Jin, S. Ergun, and B. T. Khuri-Yakub, "An efficient electrical addressing method using through-wafer vias for two-dimensional ultrasonic arrays," in *Ultrasonics Symposium, 2000 IEEE*, vol. 2, pp. 1179–1182, IEEE, 2000.

[73] X. Zhuang, A. S. Ergun, O. Oralkan, Y. Huang, I. O. Wygant, G. G. Yaralioglu, D. T. Yeh, and B. T. Khuri-Yakub, "Through-wafer trench-isolated electrical interconnects for cmut arrays," in *Ultrasonics Symposium, 2005 IEEE*, vol. 1, pp. 475–478, IEEE, 2005.

[74] X. Zhuang, A. S. Ergun, O. Oralkan, I. O. Wygant, and B. T. Khuri-Yakub, "Interconnection and packaging for 2d capacitive micromachined ultrasonic transducer arrays based on through-wafer trench isolation," in *Micro Electro Mechanical Systems, 2006. MEMS 2006 Istanbul. 19th IEEE International Conference on*, pp. 270–273, IEEE, 2006.

[75] A. S. Logan, L. L. Wong, and J. T. Yeow, "2-d cmut wafer bonded imaging arrays with a row-column addressing scheme," in *Ultrasonics Symposium (IUS), 2009 IEEE International*, pp. 984–987, IEEE, 2009.

[76] A. S. Logan, L. L. Wong, A. I. Chen, and J. T. Yeow, "A 32 x 32 element row-column addressed capacitive micromachined ultrasonic transducer," *IEEE transactions on ultrasonics, ferroelectrics, and frequency control*, vol. 58, no. 6, pp. 1266–1271, 2011.

[77] R. K. Chee, A. Sampaleanu, D. Rishi, and R. J. Zemp, "Top orthogonal to bottom electrode (tobe) 2-d cmut arrays for 3-d photoacoustic imaging," *IEEE transactions on ultrasonics, ferroelectrics, and frequency control*, vol. 61, no. 8, pp. 1393–1395, 2014.

[78] A. Sampaleanu, P. Zhang, A. Kshirsagar, W. Moussa, and R. Zemp, "Top-orthogonal-to-bottom-electrode (tobe) cmut arrays for 3-d ultrasound imaging," *IEEE transactions on ultrasonics, ferroelectrics, and frequency control*, vol. 61, no. 2, pp. 266–276, 2014.

[79] T. L. Christiansen, M. F. Rasmussen, J. P. Bagge, L. N. Moesner, J. A. Jensen, and E. V. Thomsen, "3-d imaging using row–column-addressed arrays with integrated apodizationpart ii: Transducer fabrication and experimental results," *IEEE transactions on ultrasonics, ferroelectrics, and frequency control*, vol. 62, no. 5, pp. 959–971, 2015.

[80] M. Engholm, H. Bouzari, J. A. Jensen, and E. V. Thomsen, "Capacitive substrate coupling of row-column-addressed 2-d cmut arrays," in *Ultrasonics Symposium (IUS), 2016 IEEE International*, pp. 1–4, IEEE, 2016.

[81] S. Mack, H. Baumann, U. Gösele, H. Werner, and R. Schlögl, "Analysis of bonding-related gas enclosure in micromachined cavities sealed by silicon wafer bonding," *Journal of the Electrochemical Society*, vol. 144, no. 3, pp. 1106–1111, 1997.

Appendix A

Appendix

```
/PREP7 RAD=60
CELLSP=5
SThick=2
Rfluid=750
SLength = 300
SWidth = 300
VDC = 50
TI=0.2
EPS=5.7
FG=TI/EPS
COR=50
GAP=0.2+FG
HX = SLength/5
HY = SWidth/5
FLength = 300
GLength = 600
H = 5
ET,1,SOLID45
ET,2,FLUID30,,0
ET,3,FLUID30,,1
```

ET,4,FLUID130,0

R,4,Rfluid,0,0

MP,DENS,1,2328e-18

MP,EX,1,148E3

MP,NUXY,1,0.17

MP,DENS,2,1000e-18

MP,SONC,2,1500e6

MP,DENS,3,2500e-18

MP,SONC,3,1962e6

MP,DENS,4,1055E-18

MP,SONC,4,1965e6

CYL4, 0,0,0,0, Rfluid, 90, -SThick

BLOCK, 0,SLength,0,SWidth, 0, -SThick

VPLOT

VOVLAP,1,2

NUMCMP,VOLU

SPHERE,0,Rfluid,0,90

VSBW,3

VDELE,4,,,1

VDELE,2,,,1

BLOCK,0,Rfluid,0,Rfluid,FLength,GLength,

VOVLAP,2,5

VDELE,7,,,1

VDELE,3,,,1

VGLUE,1,4,6

NUMCMP,VOLU

BLOCK,0,SLength,0,SWidth,0,GLength,

VOVLAP,2,4

VOVLAP,5,3

BLOCK,SLength,RFluid,0,SWidth,0,GLength,

VOVLAP,3,7

VOVLAP,9,4

VDELE,10,,,1

```
BLOCK,0,SLength,SWidth,RFluid,0,GLength,
VOVLAP,5,4
VOVLAP,7,11
VDELE,12,,,1
VGLUE,ALL
LSEL,S,LENGTH,,SLength
LESIZE,ALL,,,HX,1,
LSEL,ALL
LSEL,S,LENGTH,,SWidth
LESIZE,ALL,,,HY,1,
LSEL,ALL
LSEL,S,LENGTH,,SThick
LESIZE,ALL,,,1,1,
LSEL,ALL
VSEL,S,VOLU,,1
VATT,1,,1
VMESH,1
ALLSEL
VSEL,S,LOC,Z,0,FLength
VATT,2,,2
VSEL,ALL
VSEL,S,LOC,Z,FLength,GLength
VATT,3,,3
ALLSEL
VSEL,S,MAT,,3
ESIZE,30,0, !H =10
MSHAPE,0,3D
MSHKEY,1
VMESH,ALL
ALLSEL
VSEL,S,MAT,,2
ESIZE,15,0,
MSHAPE,0,3D
```

```
MSHKEY,1
VMESH,ALL
ALLSEL
ESEL,S,TYPE,,1
NSEL,EXT
ESEL,S,TYPE,,3
ESLN,R
EMODIF,ALL,TYPE,2
SF,ALL,FSI,1
NSEL,ALL
ESEL,ALL
CSYS,2
NSEL,S,LOC,X,Rfluid,Rfluid+1
CSYS,0
NSEL,R,LOC,Z,0e-6,FLength
TYPE,4
REAL,4
MAT,2
ESURF
ALLSEL
CSYS,2
NSEL,S,LOC,X,Rfluid,Rfluid+1
CSYS,0
NSEL,R,LOC,Z,FLength,GLength+1
TYPE,4
REAL,4
MAT,3
ESURF
EPLOT
ALLSEL
NSEL,S,LOC,Z,0,-SThick
NSEL,R,LOC,X,-SLength,SLength
NSEL,R,LOC,Y,-SLength,SLength
```

```
D,all,uy,0
D,all,ux,0
D,all,uz,0
NSEL,S,LOC,Z,0,-SThick
NSEL,R,LOC,X,CELLSP+0.1,CELLSP+RAD-0.1
NSEL,R,LOC,Y,CELLSP+0.1,CELLSP+RAD-0.1
DDELE,ALL,UX
DDELE,ALL,UY
DDELE,ALL,UZ
NSEL,R,LOC,Z,-SThick
CM,CELL1,NODE
NSEL,S,LOC,Z,0,-SThick
NSEL,R,LOC,X,RAD+2*CELLSP+0.1,2*CELLSP+2*RAD-0.1
NSEL,R,LOC,Y,CELLSP+0.1,CELLSP+RAD-0.1
DDELE,ALL,UX
DDELE,ALL,UY
DDELE,ALL,UZ
NSEL,R,LOC,Z,-SThick
CM,CELL2,NODE
NSEL,S,LOC,Z,0,-SThick
NSEL,R,LOC,X,3*CELLSP+2*RAD+0.1,3*CELLSP+3*RAD-0.1
NSEL,R,LOC,Y,CELLSP+0.1,CELLSP+RAD-0.1
DDELE,ALL,UX
DDELE,ALL,UY
DDELE,ALL,UZ
NSEL,R,LOC,Z,-SThick
CM,CELL3,NODE
NSEL,S,LOC,Z,0,-SThick
NSEL,R,LOC,X,4*CELLSP+3*RAD+0.1,4*CELLSP+4*RAD-0.1
NSEL,R,LOC,Y,CELLSP+0.1,CELLSP+RAD-0.1
DDELE,ALL,UX
DDELE,ALL,UY
DDELE,ALL,UZ
```

```
NSEL,R,LOC,Z,-SThick
CM,CELL4,NODE
NSEL,S,LOC,Z,0,-SThick
NSEL,R,LOC,X,CELLSP+0.1,CELLSP+RAD-0.1
NSEL,R,LOC,Y,RAD+2*CELLSP+0.1,2*CELLSP+2*RAD-0.1
DDELE,ALL,UX
DDELE,ALL,UY
DDELE,ALL,UZ
NSEL,R,LOC,Z,-SThick
CM,CELL5,NODE
NSEL,S,LOC,Z,0,-SThick
NSEL,R,LOC,X,RAD+2*CELLSP+0.1,2*CELLSP+2*RAD-0.1
NSEL,R,LOC,Y,RAD+2*CELLSP+0.1,2*CELLSP+2*RAD-0.1
DDELE,ALL,UX
DDELE,ALL,UY
DDELE,ALL,UZ
NSEL,R,LOC,Z,-SThick
CM,CELL6,NODE
NSEL,S,LOC,Z,0,-SThick
NSEL,R,LOC,X,3*CELLSP+2*RAD+0.1,3*CELLSP+3*RAD-0.1
NSEL,R,LOC,Y,RAD+2*CELLSP+0.1,2*CELLSP+2*RAD-0.1
DDELE,ALL,UX
DDELE,ALL,UY
DDELE,ALL,UZ
NSEL,R,LOC,Z,-SThick
CM,CELL7,NODE
NSEL,S,LOC,Z,0,-SThick
NSEL,R,LOC,X,4*CELLSP+3*RAD+0.1,4*CELLSP+4*RAD-0.1
NSEL,R,LOC,Y,RAD+2*CELLSP+0.1,2*CELLSP+2*RAD-0.1
DDELE,ALL,UX
DDELE,ALL,UY
DDELE,ALL,UZ
NSEL,R,LOC,Z,-SThick
```

```
CM,CELL8,NODE
CMSEL,S,CELL1,NODE
CMSEL,A,CELL2,NODE
CMSEL,A,CELL3,NODE
CMSEL,A,CELL4,NODE
CMSEL,A,CELL5,NODE
CMSEL,A,CELL6,NODE
CMSEL,A,CELL7,NODE
CMSEL,A,CELL8,NODE
CM,CELLS,NODE
EMTGEN,'CELLS','TRANS1','GROUND1','UZ',-GAP,FG,0.1
D,GROUND1,UX,0
D,GROUND1,UY,0
D,GROUND1,UZ,0
D,GROUND1,VOLT,0
ALLSEL
NSEL,S,LOC,X,0
D,all,ux,0
ALLSEL
NSEL,S,LOC,Y,0
D,all,uy,0
NSEL,ALL
/SOLU
ANTYP,0
D,CELLS,VOLT,VDC
ESEL,S,TYPE,,1
NSEL,S,EXT
NSEL,R,LOC,Z,0
sf,all,pres,0.1
allsel
ALLSELL
SOLVE
FINISH
```

```
/solu
ANTYP,HARM
HROPT,FULL
KBC,1
HARFREQ,2.4e^6
NSUBS,1
PSTRESS,ON
DDELE,CELLS,VOLT
VAC=20
D,CELLS,VOLT,VAC
ALLSEL
SOLVE
/POST1
SET,FIRST
PLNSOL, PRES,, 0,1.0
*Dim, slocat,array,120
*Dim, myarray,array,120
*Do,i,1,120,1
slocat(i)=i*5
myarray(i)=pres(node(0,0,i*5))
```

2D CMUT ARRAY BASED ULTRASONIC MICROMANIPULATION OF PARTICLES

1   **2**%

Yamaner, F. Yalcın, Xiao Zhang, and Ömer Oralkan. "A three-mask process for fabricating vacuum-sealed capacitive micromachined ultrasonic transducers using anodic bonding", IEEE Transactions on Ultrasonics Ferroelectrics and Frequency Control, 2015.
Publication

2   **1**%